Dynamics of Seawater Carbonate Chemistry in a Tropical Coastal Coral Reef Environment

By

Melissa Meléndez Oyola

Thesis submitted in partial fulfillment of the requirements for the degree of
MASTER OF SCIENCE
IN
MARINE SCIENCES
(Chemical Oceanography)
UNIVERSITY OF PUERTO RICO
MAYAGÜEZ CAMPUS
2013

Approved by:

_____	_____
Julio M. Morell, M.S. Member, Graduate Committee	Date
_____	_____
Wilson Ramirez, Ph.D. Member, Graduate Committee	Date
_____	_____
Jorge E. Corredor, Ph.D. Chairman, Graduate Committee	Date
_____	_____
Kurt Grove, Ph.D. Representative, Graduate Studies	Date
_____	_____
John Kubaryk, Ph. D. Chairperson of the Department	Date

Abstract

Diverse forcing such as biogenic and abiogenic calcification, carbonate sediment dissolution or precipitation, and climate-related processes modulate seawater carbonate equilibrium and Ca^{2+} and Mg^{2+} proportions in near coastal coral reef environments. To this end, we characterized seasonal and inter-annual carbonate dynamics from 2009 to 2012 in the coral reef ecosystem of La Parguera, Puerto Rico. Additionally, we implemented a method for the quantification of seawater Ca^{2+} and Mg^{2+} concentrations using High Performance Chelation Ion Chromatography. The new method, as implemented, achieves a precision of 2 %. Although we have not yet achieved the chromatographic precision required for seawater calcification applications, the method was applied to marine sediment porewaters where acid dissolution results in excess Ca^{2+} and Mg^{2+} concentrations. Carbonate saturation state at the reef showed seasonal depressions. Differential total inorganic carbon and total alkalinity indicate that calcification and photosynthesis are thus the major processes controlling carbonate chemistry at Enrique reef.

Keywords: *calcium, magnesium, carbonate chemistry, marine porewaters, chelation ion chromatography, La Parguera Marine Reserve*.

Resumen

Diversos procesos tales como la calcificación, disolución o precipitación en los sedimentos marinos y procesos climáticos relacionados, modulan el equilibrio en la química de carbonatos y las proporciones de Ca^{2+}/ Mg^{2+} en los ambientes de arrecife costeros. Se caracterizó la dinámica de carbonatos estacional e interanual desde el 2009 al 2012 en el ecosistema de arrecifes de coral en La Parguera, Puerto Rico. Además, se implementó un método para la cuantificación de las concentraciones de Ca^{2+}/ Mg^{2+} en agua de mar utilizando cromatografía de quelación iónica de alta eficacia. El método se aplicó utilizando agua intersticial de sedimentos marinos en donde la disolución resulta en un exceso de Ca^{2+}/ Mg^{2+}. Se observaron disminuciones estacionales en el estado de saturación de carbonato. Cambios en carbono inorgánico total y alcalinidad total indican que la calcificación y la fotosíntesis son los principales procesos que controlan la química de carbonato de Cayo Enrique.

Palabras claves: *calcio, magnesio, química de carbonatos, aguas intersticial marina, cromatografía de quelación iónica, Reserva Marina de La Parguera.*

Dedication

This thesis is dedicated to the memory of Godoberto López (Godo).

Acknowledgements

I would like to give special thanks to Dr. Jorge E. Corredor, Prof. Julio Morell, and Dr. Wilson Ramírez for the opportunity of working with them and their advice throughout the development of this thesis. I also thank Dr. Dwight Gledhill, Dr. Wade McGillis, Dr. Brice Loose, and Dr. Chris Langdon for their advice and recommendations throughout the MapCO_2 operations. Special thanks to the Australian Centre for Research on Separation Science (ACROSS) and Dr. Pavel Nesterenko for their support, advice and hospitality at University of Tasmania (UTAS), Australia. Thanks to Belitza Brocco, Val Hensley, Anibal Santiago, and Eduardo Mercado for field and lab assistance. I would like to thank the family of Godoberto López for understand all the extra hours that he spent with me and other students working in "La Mar". Many thank the staff of the Department of Marine Sciences for always helping me.

I cannot forget to give my deepest gratitude to my family and friends for their support, love, patience, and for always being there.

Support for this study was provided in by the NOAA IOOS Caribbean Coastal Ocean Observing System (CariCOOS), NOAA Coral Reef Conservation Program (CRCP), Sea Grant Puerto Rico, ExonMobil, Department of Marine Science (DMS) UPR-M, UTAS, and ACROSS. La Parguera MapCO_2 buoy and data analysis was possible thanks to the join effort between Pacific Marine Environmental Laboratory (PMEL), Atlantic Oceanography and Meteorological Laboratory (AOML), NOAA's Coral Health and Monitoring Program, and Ocean Acidification Project. MapCO_2 support was provided thank to the CRCP who paid for the initial deployment and servicing cost.

Table of Contents

List of Tables

List of Figures

List of Appendixes

Introduction

1.1 Ocean Acidification Global Trends

Increased emission of carbon dioxide (CO_2), one of the major greenhouse gases in the atmosphere produced by the burning of fossil fuels, is expected to produce changes in ocean chemistry that may affect marine life (Mackenzie et al. 2001). Since the onset of the industrial revolution, the global ocean has served as a major sink of anthropogenic CO_2 (Mackenzie et al. 2001; Sabine et al. 2004). Kleypas et al. (2006) and Ruttimann (2006) estimated that in 1800 the CO_2 concentration in the atmosphere was 280 parts per million (ppm), and the global ocean pH averaged 8.16. Currently, atmospheric CO_2 concentration has reached 400 ppm, (Dlugokencky & Tans, n.d.) and the average pH of the surface oceans has dropped to 8.05 (IPPC 2007). Moreover, the Global Carbon Project (2008) reported that carbon emissions increased 2.9 % from 2006 to 2007, and by 29% between 2000 and 2008 (Le Quéré et al. 2009). Since the Industrial Revolution, CO_2 concentration has increased by about 35% and pH has decreased by 0.1 units (IPCC 2007). The oceans are currently taking up about one ton of anthropogenic CO_2 per year for each person on the planet (IPCC 2001). If atmospheric CO_2 concentration continues increasing, by the next century the average pH of oceanic waters will decrease by 0.3 – 0.4 units below the level of pre-industrial times (Kleypas et al. 2006; Ruttimann, 2006). These rapid changes do not allow for natural adaptation to occur in ecosystems that have experienced only moderate changes in ocean chemistry over most of geological time (The Royal Society, 2005).

The current rate of change in ocean chemistry due to the rapid increase in atmospheric CO_2 concentration is expected to affect ocean ecosystems within the coming decades and centuries (Guinotte & Fabry, 2008). Ocean acidification may be defined as the change in ocean

chemistry when CO_2 from the atmosphere dissolves in seawater reacting with water to produce carbonic acid (H_2CO_3) (Kleypas et al. 1999, 2006; Andersson et al. 2003, 2005, 2007; Orr et al. 2005; Morse et al. 2006; Atkinson & Cuet, 2008; Guinotte & Fabry, 2008). Carbonic acid rapidly dissociates and causes an increase in hydrogen ions (H^+) and bicarbonate (HCO_3^-), while simultaneously causing a decrease, carbonate (CO_3^{2-}) concentration, and the saturation state of seawater with respect to calcium carbonate minerals (Kleypas et al. 1999, 2006; Andersson et al. 2005; Orr et al. 2005; Morse et al. 2006). This chemical process is summarized as follows (Morse & Mackenzie, 1990; Zeebe & Wolf-Gladrow, 2001; Andersson et al. 2003, 2007; Hönisch et al. 2012):

$$CO_2 + H_2O \leftrightarrow H_2CO_3 \leftrightarrow H^+ + HCO_3^- \leftrightarrow 2H^+ + CO_3^{2-} \quad (1)$$

As a result of the decrease in seawater carbonate saturation state, the rate of biotic and abiotic calcification decreases as well (Caldeira & Wickett, 2003; Kleypas et al. 2006; Andersson et al. 2007; Atkinson & Cuet, 2008). The seawater saturation state is calculated as:

$$\Omega = [Ca^{+2}][CO_3^{2-}]/K*_{SP} \quad (2)$$

where Ω indicates the degree of carbonate saturation with respect to calcium carbonate mineral phase and $K*_{SP}$ is the stoichiometric solubility product constant (Andersson et al. 2005, 2007; Kleypas et al. 2006; Atkinson & Cuet, 2008; Guinotte & Fabry, 2008). If Ω is equal to one, the seawater is said to be in equilibrium; if Ω is greater than one, the seawater is supersaturated; and if Ω is less than one, the seawater is undersaturated. Thermodynamically, undersaturation implies that the mineral phase could be subject to net dissolution (Andersson et al. 2007).

As carbonate minerals are the principal components used by marine calcifying organisms to produce their internal and external skeletons, some of the most fundamental biological and

geochemical properties and processes such as marine calcification rates, physical strength of calcareous skeletons of corals reef, shell growth, recruitment success, reproduction, survivorship, and food web dynamics in general (Kleypas et al. 2006; Morse et al. 2006; Andersson et al. 2007) may be adversely affected by a decrease in the availability of carbonate ions. As a result, species that undergo calcification may become displaced by species that do not. By some estimates, calcification rates for various calcareous marine organisms will decrease as much as 60% by the end of this century (Ruttimann, 2006). Currently, in the tropics the aragonite saturation state of surface seawater ranges from 3 to 3.5 and it is expected to decrease for the next century near 2 to 2.5 (Orr et al. 2005; Atkinson & Cuet, 2008). Laboratory experiments have conclusively shown that lowering carbonate ion concentration reduces calcification rates in tropical reef builders by 7–40% (Gattuso et al. 1999; Langdon et al. 2000, 2003; Marubini et al. 2003).

1.2 Mg-calcites and Ca^{2+} and Mg^{2+} seawater concentrations

In the open ocean, variations of Ca^{2+} and Mg^{2+} ion concentrations are rather small and respond for the most part to changes in salinity. The estimated Ca^{2+}: salinity ratio for the open oceans varies by about 1.5% (Feely et al. 2004). However, in the coastal zone where spatial and temporal heterogeneity are significant, changes in Ca^{2+}, Mg^{2+} and CO_3^{2-} seawater concentrations arise from the precipitation or dissolution of carbonate minerals (Koczy, 1956; Traganza & Szabo, 1967; Kanamori & Ikegami, 1980; Kleypas et al. 2006; Ribou et al. 2007).

Aragonite, calcite, high and low Mg-calcite, and dolomite minerals comprise the vast majority of carbonate minerals found in ocean sediments and sedimentary rocks (Berner, 2004). The most soluble are aragonite and Mg-calcites. The Mg-calcites are divided into two mineral

phases based on the mol% of $MgCO_3$. Those with low mol% $MgCO_3$ (< 4 mol%) are the least soluble phase (Reeder, 1983; Mackenzie et al. 1983; Morse et al. 2006; Andersson et al. 2008). In contrast, Mg-calcites with high mol% $MgCO_3$ (> 4 mol% $MgCO_3$) will be the "first responders" to a decrease of pH and Ω due to their high solubility (Morse et al. 2006; Andersson et al. 2008). Changes in Ω with respect to Mg-carbonate phases are not only affected by changes in the CO_3^{2-} concentration. Variations in the Ca^{2+} and Mg^{2+} seawater concentrations and their ratio imply changes in Mg-calcite composition, magnesium content of calcitic skeletons as well as changes in saturation state (Andersson et al. 2008). Precipitation of lower magnesium content calcite is facilitated, both kinetically and thermodynamically, under decreased Ω (Mackenzie et al. 1983; Stanley et al. 2002; Andersson et al. 2008). In addition, different ways of incorporation of Mg^{2+} in marine calcite minerals will cause changes in the solubility of these calcium carbonate mineral forms.

The effects of ocean acidification on the Mg-calcite mineral phase is not well understood due to problems involving the precision of measurements and uncertainty regarding the basic thermodynamic solubility and kinetic properties of this phase (Morse et al. 2006). Direct determination of Ca^{2+} and Mg^{2+} concentrations can help in better understanding the chemical behavior of these metastable carbonate mineral phases and in more accurate determination of their corresponding Ω (Kleypas et al. 2006; Ribou et al. 2007).

The alkaline earth metals Ca^{2+} and Mg^{2+} are part of the major solutes in seawater, thus their high concentration and the complexities of the matrix make them very troublesome to high-precision determination (Traganza & Szabo, 1967; Kanamori & Ikegami, 1980). Dittmar on 1984 first described the Ca^{2+} anomalies due to the changes in seawater alkalinity. The delicate

equilibrium between these two alkaline earth metal cations is triggered by slight changes in alkalinity and carbon dioxide tension that may cause their precipitation (Irving, 1926). Seawater Mg^{2+} concentration is not usually directly determined due to the precision difficulties and is usually determined by the difference between total alkaline earth metals and Ca^{2+} plus strontium (Kanamori & Ikegami, 1980). The direct determination of these ions in seawater is important in order to investigate the chemical equilibrium between them and their relationship with changes in seawater CO_3^{2-} ion concentration. It has been estimated (Kanamori & Ikegami, 1980; Olson & Chen, 1982) that, in order to establish small variations in Ca^{2+} and Mg^{2+} concentrations due to biotic and abiotic processes in coastal seawaters we need determine the seawater concentration of these two ions with an error of less than 0.1% level.

1.3 Carbonate dissolution in sediment porewaters

The chemical composition of the sedimentary environment changes due to the utilization and production of geochemically reactive species and the alteration of the geochemical environment (Mills, 1999). Respiration by metabolic processes releases CO_2 which reacts with water (Eq. 3), increasing both the alkalinity and total dissolved inorganic carbon (DIC). This increase is assuming that the alkalinity added by N and P remineralization and the acid productions associated with the oxidation of metal sulfides such as FeS are neglected. Burdige & Zimmerman (2002) noted that production of acid by aerobic respiration, and therefore the consumption of CO_3^{2-} ions, decreases the Ω of the most soluble carbonate mineral phases in sediment porewaters. The total reaction process is summarized as:

$$CH_2O + O_2 + CaCO_3 \rightarrow Ca^{2+} + 2HCO_3^- \quad (3)$$

Organic matter remineralization processes and the metabolic CO_2 production force carbonate dissolution in aerobic surface layers of the carbonate sand marine sediments (Burdige & Zimmerman, 2002; Andersson et al. 2006). When aerobic processes deplete the oxygen available in sediments, anaerobic microorganisms use other chemical species as alternate oxidants and other reactions control the chemistry of sediment pore waters (e.g. reduction of oxidized metabolites). Bacterial utilization or production of oxidized or reduced chemical species may cause further large redox shifts causing corresponding shifts in pH (Mills, 1999), TA and DIC. However, under aerobic conditions and constant salinity, carbonate dissolution and biogenic precipitation of calcium carbonate are the dominant processes affecting TA in seawater (Zeebe & Wolf-Gladrow, 2001; Andersson et al. 2007).

1.4 Changes in Carbonate Chemistry

Over longer periods (> 10^5 years) of increasing CO_2 concentrations (Caldeira & Berner, 1999), dissolution of meta-stable carbonate mineral phases, such as high Mg-calcite and aragonite, could renew the ocean's buffering ability and re-establish its chemical behavior (Caldeira & Wickett, 2003; Andersson et al. 2003, 2007). This change is due to the consumption of one molecule of CO_2 by the dissolution of carbonate minerals to produce two ions of bicarbonate and calcium ion, thereby increasing the seawater total alkalinity (TA) according to the following reaction (Morse et al. 2006):

$$CO_2 + H_2O + CaCO_3 \rightarrow Ca^{2+} + 2HCO_3^- \quad (4)$$

Andersson et al. (2003) concluded, based on modeling results, that meta-stable carbonate minerals could dissolve in the future, but the surface water of the global shallow-water marine

environment will not accumulate sufficient alkalinity to buffer pH or carbonate saturation state significantly on time scales of decades to hundreds of years. Seawater TA is described as follows (Zeebe & Wolf-Gladrow, 2001; Andersson et al. 2007):

$$TA = [HCO_3^-] + 2[CO_3^{2-}] + [B(OH)_4^-] + [OH^-] - [H^+] + minor\ constituents \\ = [Na^+] + 2[Mg^{2+}] + 2[Ca^{2+}] + [K^+] - [Cl^-] - 2[SO_4^{2-}] \quad (5)$$

The future precipitation events and the increase in river runoff due to the effects of climate change could have a significant effect on carbonate chemistry in the Caribbean Region. The oligotrophic Caribbean Surface Water mass (CSW) originates in the passages between the Antilles islands connecting the western tropical Atlantic Ocean with the Caribbean Sea. The Orinoco and Amazon River plumes play an important role in reducing CSW salinity between the months of May and October (Corredor & Morell, 2001). The Orinoco River plume in particular extends seasonally approximately 1,000 km from the Gulf of Paria throughout the eastern Caribbean Sea. Froelich et al. (1979) and Navarro et al. (2000) documented NE Caribbean CSW salinity depressions from 36; typical of surface waters in the western tropical Atlantic to values as low as 33. Resulting changes in biotic and abiotic parameters and processes (e.g. primary productivity, mineralization, nutrient concentrations, dissolved organic matter (DOM), temperature, salinity, dissolution, calcification, photosynthesis, and respiration) therefore, affect carbonate chemistry in general (e.g. DIC, pH, TA, pCO_2, and Ω). Seasonal evaporation, rainfall, and local runoff in the vicinity of islands in the NE Caribbean further affect CSW salinity and thus TA.

Objectives

This work focuses on the differences between offshore surface reference waters and the waters within the coral reef environment including overlying shelf waters and sediment porewaters at La Parguera Marine Reserve. In this context, the objectives of the study are to:

1) develop a method to determine both Ca^{2+} and Mg^{2+} concentrations in seawater (refer to Appendix 1);

2) determine seawater Ca^{2+} and Mg^{2+} concentrations in porewaters and seawater;

3) determine the precision of seawater Ca^{2+} measurements necessary to discern drawdown by shelf calcifiers;

4) estimate carbonate mineral dissolution rates in the sediment porewaters; and

5) characterize seasonality of the carbonate system.

Materials and Methods

1.5 Site Descriptions

The town of La Parguera (17° 58' 19.10" N, 67° 02' 42.50" W) is located on the southwest coast of Puerto Rico. While the hurricane season covers from June to September the rainy season extends between May to October; the rest of the year semiarid weather prevails (February, March and April are the driest months). The insular shelf extends out up to 8 km from the coast (Morelock et al. 1977). The Marine Protected Area of La Parguera covers an area of ~50 km^2 (Protected Areas Database compiled by United Nations Environment Programme - World Conservation Monitoring Centre (UNEP-WCMC)). Shelf depths range from 15 to 20 m from inshore to the shelf break (Hubbard et al. 2008). Shelf sediments are comprised of biogenic

carbonate material and terrigenous (<10%) (Morelock et al. 2001). Sediment sizes comprise silt and clays. The major sand contributors are fragments of *Halimeda,* coralline algae, corals, foraminifers, and mollusks. The major coral species present in shallow areas are *Porites porites, Acropora palmata* and *Montastraea annularis*. In the mid and deeper parts *Acropora cervicornis, Montastraea spp., Diploria spp, Agaricites spp., Manicina areolata, Mycetophyllia spp*., and *Scolymia spp.* are common.

The shelf in La Parguera is divided in different regions according to its general morphological and depositional characteristics. The inner shelf is approximately 1-2 km offshore and extends from the coast to Enrique coral reef. The mid-shelf reefs are ~ 2-4 km offshore and are associated with submerged shoals and include Laurel, Media Luna, Enrique, and Corral coral reefs. This section is associated with muddier shoals and rubble islands. The shelf-edge reefs, located at 20 m depth comprise a marginal barrier reef ~8 km offshore (Morelock et al. 1977).

1.6 Sampling Stations

The offshore station (17.87 N, -67.02 W) is located 1.6 km south (seaward) of the shelf-edge at a depth of approximately 500 m. Characteristics of individual inshore stations chosen for this study are discussed below.

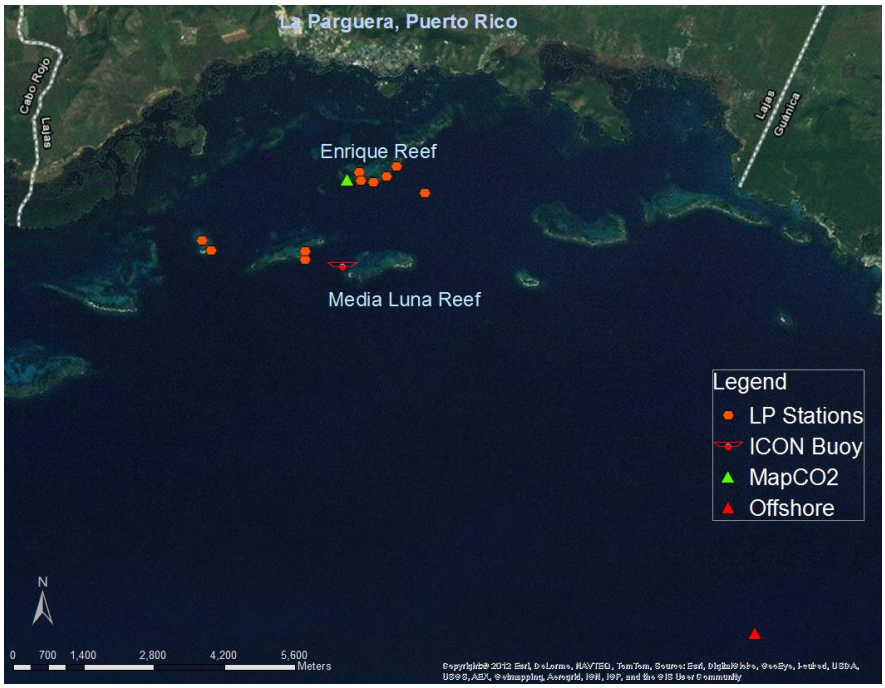

Figure 1: Sample stations near La Parguera located along the southwestern coast of Puerto Rico (orange circles). The MapCO$_2$ station (green triangle) represents the inshore reef station. The offshore station (red triangle) is ~1.6 km from the shelf-edge reef. The ICON station (red moored buoy icon) is located at Media Luna reef.

The inshore station is at Enrique mid-shelf reef (17.95 N, -67.05 W) located at 2.5 km from the coast and 11.5 km from the offshore station (Figure 1). The average depth ranges from 1 m at the reef flat to 21 m at the forereef (Morelock et al. 1977). The average ocean current at Enrique reef is from 2 to 10 cm s^{-1} towards the west (McGillis et al. 2011). A lagoon sandy area with *Thalassia* beds, and a few areas of patch reefs are located at the back reef and reef flat. The average sediment sizes are from medium to coarse-grained and poorly to moderately sorted sands (Morelock et al. 1977). The carbonate sand source is principally from *Acropora spp. and Porites spp.* corals (40 to 80%), coralline-algae (10 to 20%), and *Halimeda* fragments (Morelock et al. 1977).

Enrique forereef and upper zone reef communities were formerly dominated by branching growth forms of *Acropora palmata*. Over the last three decades significant loss of coral live tissue cover and abundance has been in decline. The combined effects of primarily from hurricane damage, coral diseases, corallivorous mollusks (Morelock et al. 2001), die off of *Diadema antillarum*, and mass coral bleaching events are notable processes contributing to this lost. McGillis et al. (2011) noted during belt transects surveys only 10 % live coral cover area. The stony coral species observed were *Siderastrea siderea, P. astreoides, Diploria strigosa, S. radians, D. clivosa,* and *P. porites* ranked in order of areal cover. Soft corals are also present, such a *Gorgonia spp*. and *Psuedoterigorgia spp.* (Morelock et al. 2001). Nowadays, most of the area covered by *Acropora palmata* is dead and replaced by *Milleropa spp., Diploria spp.*, and the zoanthids, *Palythoa carribberaum*.

1.7 Carbonate chemistry measurements

Complementary chemical, physical, and meteorological measurements monitored within the La Parguera Marine Reserve are used to track the dynamics and controls on local carbon chemistry. A moored autonomous pCO_2 system (MapCO_2) is deployed over the forereef of the Enrique mid-shelf reef (Figure 2). The autonomous capability of the MapCO_2 buoy provides continuous 3 hourly measurements of both air and dissolved CO_2 mole fraction along with temperature, salinity, and dissolved oxygen. The data are transmitted daily for quality control to NOAA PMEL (more information at: http://pmel.noaa.gov/co2/story/La+Parguera). These autonomous observations are validated and supplemented on a weekly basis through discrete sampling. Bi-weekly surface water samples are collected along Enrique forereef (orange circles, Figure 1), at the MapCO_2 site (green triangle), and 11 km offshore from the MapCO_2 in deep

waters 1.6 km off the insular shelf-edge (red triangle). Profile measurements of chemical and physical parameters are continually taken using a SBE25® conductivity, temperature, and depth recorder (CTD). Seawater samples are collected using a Van Dorn type sampler bottle at the surface (0 m) and near bottom (approximately 3 m). The seawater samples are drawn from the sampler into 250 mL Biological Oxygen Demand (BOD) flasks and stored at room temperature for analysis of TA and spectrophotometric pH within 24 hours. The pH samples are analyzed using a UV-VIS spectrophotometer (Shimadzu UV-1601) and metacresol purple as indicator (Cullison, 2010) according to the DOE procedures (DOE, 1994). The precision of the method as implemented is ±0.006. TA seawater analysis is performed using a potentiometric acid titration system. The Certified Reference Materials (CRMs) of Dickson et al. (2003) are used to standardize the nominal 0.1 M hydrochloric acid (HCl) titrant. The potentiometric acid titration system is a custom-built Gran titration system (for details see Langdon et al. (2000)). Precision of the method as implemented is ±1.12 μequiv kg^{-1}_{SW}. If TA and pH analyses are not accomplished within 24 hr of sampling, each sample is poisoned with a saturated solution of mercuric chloride ($HgCl_2$; 100 μl) to prevent biological alteration of the sample (Dickson et al. 2007). Each bottle is assured of a tight seal in order to prevent atmospheric gas exchange. Approximately 45 mL of seawater samples are filtered through 0.2μm membrane filters and stored in refrigerator for the Ca and Mg analysis (details on Appendix 1).

Figure 2: The MapCO$_2$ buoy deployed at Enrique mid shelf reef provides measurements of atmosphere and seawater CO$_2$ mole fraction, seawater temperature and salinity at 3-hour intervals (photo by Gledhill, D.).

The CO_2 system is solved using the program CO_2SYS from Lewis et al. (1998) and adapted to Excel by Pierrot et al. (2006) applying the dissociation constants for K_1 and K_2 of Mehrbach et al. (1973) reformulated by Dickson & Millero (1987), and for K_{HSO4-} from Dickson (1990). The solubility constant used to derive Ω_{arg} is from Mucci (1983).

The CO_2 flux between ocean and atmosphere, driven by differences in fCO_2 at the air – sea interface is parameterized according to Bates et al. (2001) through the expression:

$$F_{CO2} = ks\,(fCO_2) \tag{6}$$

where F is the net air-sea flux (mmoles CO_2 m^{-2} d^{-1}), s is the solubility of CO_2 per unit volume of seawater (Weiss, 1974), and k is the transfer velocity as a function of wind speed. The transfer velocity-wind speed relationship described by Wanninkhof (1992) is used:

$$k = 0.31u^2(660/Sc)^{1/2} \tag{7}$$

where u is the wind speed at 10 m above mean sea level. Wind speed was obtained from the nearby ICON/CREWS station, located at Media Luna shelf reef (17° 56' 19" N, 67° 3' 7" W) at ~ 3.3 km from the coast and ~1.8 km from the MapCO$_2$ buoy (Figure 1), and provides continuous near real-time meteorology data since 2006

(http://ecoforecast.coral.noaa.gov/index/0/LPPR1/station-data). The Sc is the CO_2 Schmidt number calculated from Wanninkhof (1992).

1.8 Calcium and Magnesium Analysis

A method for the detection and quantification of both Ca^{2+} and Mg^{2+} ion concentrations in seawater was developed and implemented at the UPR-M Magueyes Island laboratories and refined at the Australian Centre for Research on Separation Science (ACROSS) under the supervision of Dr. Nesterenko, Professor in the Chemistry School at University of Tasmania, Australia (details on Appendix 1). The Ca^{2+} and Mg^{2+} ion concentrations were accurately determined using High Performance Liquid Chelation Ion Chromatography (HPLCIC), a post column flowing reaction system, and spectrophotometric detection of the resulting colored Ca and Mg ion chelates (Figure 3).

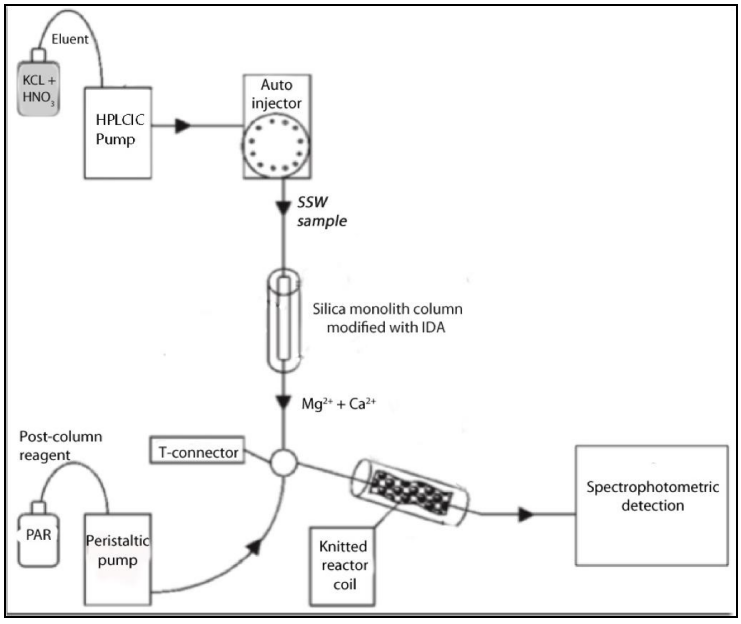

Figure 3: Schematic design of the HPLCIC system used. Figure modified from Aura Industries, Inc.

1.8.1 Monolithic silica IDA modified column

A monolithic bare silica column (Phenomenex 100 x 4.6 mm) was modified with IDA chelator through the activation of silanol groups at the surface of the silica monolith column with distilled water (DW) at 60 °C followed by recycling of mixture IDA and 3-glycidoxypropyltriethoxysilane through the column at 70 °C (for method details see Sugrue et al. 2003; Nesterenko & Jones, 2007; Nesterenko et al. 2012). Surface treatment and functionalisation of the continuous unitary porous structure and structure of the bonded layer within such columns have been described by Sugrue et al. (2004) and Nesterenko et al. (2012).

1.8.2 Reagents and Solutions

For photometric detection, we used PAR reagent (CAS# 1141-59-9, acid form – Fluka, 99% purity) as a post-column reagent. We prepared stock solutions of 1 mM PAR and 2 M ammonia (analytical reagent grade). The ammonia is necessary to ensure the pH of the stock solution is close to 10 to prevent adsorption onto the plastic surfaces. The standard post column reagent was prepared by dilution to 0.05 mM PAR. To adjust the pH to ~10.4 we used 2 M nitric acid (analytical reagent grade). The post-column reagent thus prepared is stable for weeks if not months, and will not need filtering, degassing or an overpressure of inert gas.

The mobile phase was prepared using 0.1 M potassium chloride (KCl) and 1 mM HNO_3, pH of ~2.5. Standard seawater (International Association for the Physical Sciences of the Ocean – IAPSO, batch 149; 5/10/2007) with salinity 34.994 was purchased from OSIL (Havant, UK). Stoichiometric reference composition of IAPSO standard seawater provides the best current estimation of Mg^{2+} (0.05474 mol kg^{-1}) and Ca^{2+} (0.01065 mol kg^{-1}) concentrations in seawater (Millero et al. 2008).

We used Nalgene bottles for storage of all stock and working solutions since prolonged soak in nitric acid was not required due to the low metal contamination of Nalgene. Glassware and plasticware were acid washed before use with 10 ml of 1 M nitric acid (shaken for 1 minute with tap) followed by a rinse with deionized water provided form a Milli-Q system (Millipore, Bedford, USA).

1.8.3 Chromatographic Instrumentation

A Waters 2695 HPLC Separations Module (Waters, Milford, MA, USA) chromatography system was used. The autosampler built in to the Separation Module allowed runs of 178 samples in a single analytical sequence. Column oven was set to 30 ^{o}C for all separations. A post column reaction (PCR) flow system was used to allow cation detection. The 1/16" polypropylene mixing coil used in the PCR was about 2.5 m long using a high-pressure pump model 350 (Scientific System Inc., State College, PA, USA). The colored PAR-derivatized cations were detected spectrophotometricaly using a model 2487 UV/VIS spectrophotometric detector operated at 510 nm. Data was processed using the Waters Empower 3 Integration Software.

1.9 Porewater samples

1.9.1 Porewater well samplers and sampling techniques

In order to study carbonate dissolution processes within reef sediments at Enrique mid-shelf reef, stainless steel well samplers (3/4" i.d.) were developed which allow porewater sampling down to 25 cm sediment depth (Figure 4). Each sampler is placed 1 m apart on a 10 m transect along the reef. Each sampling port consists of thirty 1/16-inch holes drilled around the

sample in a 1 cm span (Figure 4). Samples were taken at 2 cm resolution through the upper 20 cm of the sediment. Following the technique presented by Falter & Sansone (2000) we installed the samplers by first hammering a stainless steel tube (54 cm long, 5/8" i.d.) into the sediment and then replacing it with the well sampler (Figure 5). After insertion into the sediment, the sampler is left on site allowing repetitive sampling at identical locations and depth intervals. The first samples were collected after two weeks of the insertion of the samplers into the sediment to equilibrate the system. The water sample is collected in situ by withdrawing porewater using two 60cc syringes and storing in 125 mL plastic sample bottles. Sample volume limitation precludes DIC and pH, thus gas exchange does not represent a problem in this case. Each sample is filtered immediately through 0.45μm membrane filters and poisoned with $HgCl_2$; 60 μl. Porewater samples were analyzed for TA, Ca^{2+}, and Mg^{2+} seawater ion concentrations. Porewater samples for salinity are taken and analyzed using a salinometer (Autosal Guildline, 8400B) with a precision of ± 0.003. CTD casts of the overlying water column are routinely performed. Surface and bottom samples of the overlying seawater are collected for TA and Ca^{2+} and Mg^{2+} analyses as well, using a Van Dorn type bottle.

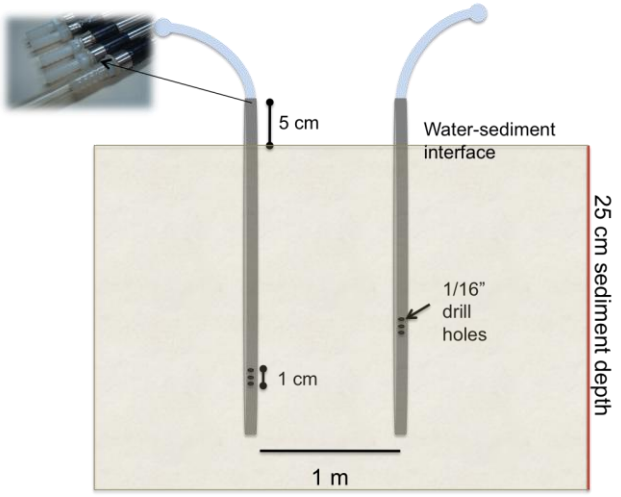

Figure 4: Sediment samplers used. Special precautions were taken in order to avoid dead space between the connections.

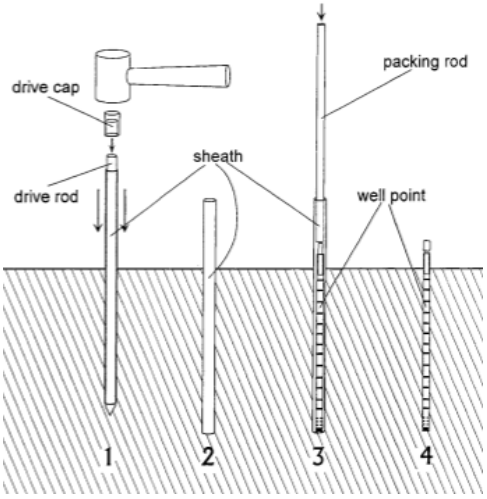

Figure 5: Schematic design of the sediment sampler installation tool using a drive rod and sheath. A stainless steel tube is drawn into the sediment using the drive rod and a hammer. The drive rod is driven out of the sediment and the well is in place. After insertion into the sediment the sheath is removed and the sampler stays on site allowing repetitive sampling at identical locations and depth intervals. Design and figure are after Falter & Sansone (2000).

1.9.2 Calculation of Vertical Diffusion and Carbonate Dissolution Rates

The vertical diffusive flux of TA (F_{TA}) (mmol m^{-2} h^{-1}) normalized to a fixed salinity (S=35) is calculated in order to estimate the calcium carbonate dissolution rates in carbonate

porewaters. F_{TA} is calculated according to Fick's First Law using diffusivity in seawater as described by Andersson et al. (2007):

$$F_{TA} = -D \times dTA/dz \quad (8)$$

where D is the diffusion coefficient ($m^2\ s^{-1}$) in the vertical direction and dTA/dz denotes the concentration gradient of TA. The porosity (ϕ) is estimated gravimetrically. The porosity of carbonate sediments normally range between 40% and 70% (Enos & Sawatsky, 1981). The diffusion coefficient is estimated using Archie's Law (Berner, 1980) as:

$$D_s = D_0/\phi^{m-1} \quad (9)$$

where D_s is the bulk sediment diffusion coefficient of the solute in ($m^2\ s^{-1}$), D_o is the free solution diffusion coefficient of solute ($m^2\ s^{-1}$) corrected for temperature and pressure (Li & Gregory, 1974). The bicarbonate diffusion coefficient was used. The relationship between D_s, ϕ, and the formation resistivity factor of porous sediment is described by Archie (1942), Berner (1980), and Ullman & Aller (1982). As noted by Ullman & Aller (1982), *m* ranges 1.3 - 2 for sands and sandstones. Particular precautions need be taken in order to decrease the possibility of under or sub estimating D_s. Thus, we estimate *m* from geometric correction factors based on porosity ($\phi \approx 0.7 - 0.9$, m value is around 2.5 to 3; and for $\phi \leq 0.7$, the *m* value is 2).

The bulk porosity of the sandy sediment is determined on samples collected with a sediment core of about 750 cm^3 (15 cm long and 8 cm wide). The samples are placed in pre-weighed ceramic crucibles (about 30 cm^3) and weighed for the determination of sediment porosity and water content. To achieve complete dryness, the crucible remains in a muffle

furnace (Thermolyne Sybron 1300) for two days at 80 °C. Precautions are taken to avoid absorption of atmospheric humidity by the dried sample until weighed.

The rates of calcium carbonate dissolution (R_{CaCO3}) are estimated using the vertical diffusive flux of TA and which, in accordance with equation 4, can be described as:

$$R_{CaCO3} = F_{TA}\frac{1}{2} \tag{10}$$

where R_{CaCO3} is in units of mmol $CaCO_3$ m^{-2} h^{-1}.

Results

1.10 Characterization of the seasonality of the carbonate system at La Parguera Marine Reserve from 2009 to 2012

The mean seawater surface temperature (SST) from 2009 to 2012 was 28.5 ± 1.24 ˚C. SST at the MapCO_2 buoy ranged from 25.9 to 31.7 ˚C. The highest SST recorded throughout the 4 annual cycles occurred in August of 2010. The lowest SST was observed during the 2009 wintertime (Figure 6). The mean seawater surface salinity (SSS) observed on Enrique mid-shelf reef at the MapCO_2 buoy between 2009 and 2012 was 35.3 ± 0.592 (n=9707). Freshwater input from the Amazon and Orinoco River plumes as well as increased local rainfall caused recurrent decrease in salinity during the months of June through October. A minimum SSS value of 31.9 was recorded in October 2010 at the MapCO_2 buoy site. Responding to decreased precipitation and increased evaporation, salinity typically increases during the spring months (March to June). A maximum SSS value of 36.4 was recorded in May 2009 (Figure 6). Air and seawater CO_2 fugacity (a measure close to partial pressure of CO_2 in applications that do not require precision

> 0.7%) increases during the summer. The mean seawater and air fCO_2 values from 2009 to 2012 were 420 ± 27.0 and 382 ± 9.26 μatm (n=9707), respectively. Maximum seawater fCO_2 values were observed in summer and fall and minima occurred in the spring. In contrast, air fCO_2 fluctuations were much more modest. Maxima were observed in the spring and minimum in the summer. The mean air-sea difference in fCO_2 from 2009 to 2012 was 38.4 ± 29.9 μatm (n=9707). Maximum and minimum differences in fCO_2 were 156 and -52.3 μatm, respectively (Figure 6). CO_2 flux at Enrique reef ranged from about -5 to 30 mmoles CO_2 m^{-2} d^{-1} between January 2009 and October 2011 (Figure 7, wind speed measurements not available for 2012 at the ICON cruise buoy). The maximum CO_2 fluxes were in summer and fall and lowest fluxes were registered in winter and spring.

Phosphate and silicate concentrations were measured 6 times during 2009 to 2011 on the months of January, February, March, May, November, and December at reef and offshore sampling stations. The monthly averages for phosphate and silicate at the reef and offshore stations were 0.032 ± 0.018 μmol L^{-1} and 1.83 ± 0.277 μmol L^{-1}; and 0.016 ± 0.017 μmol L^{-1} and 1.69 ± 0.252 μmol L^{-1}, respectively. Corredor et al. (unpublished data) measured silicate and phosphorous monthly at the Caribbean Time Series station (CaTS) for 4 years from 2002 to 2005 and reported mean near surface values for these nutrients of 1.71 ± 0.131 μmol L^{-1} and 0.011 ± 0.005 μmol L^{-1}, respectively. The contribution to TA of phosphate and silicate at these concentrations is negligible.

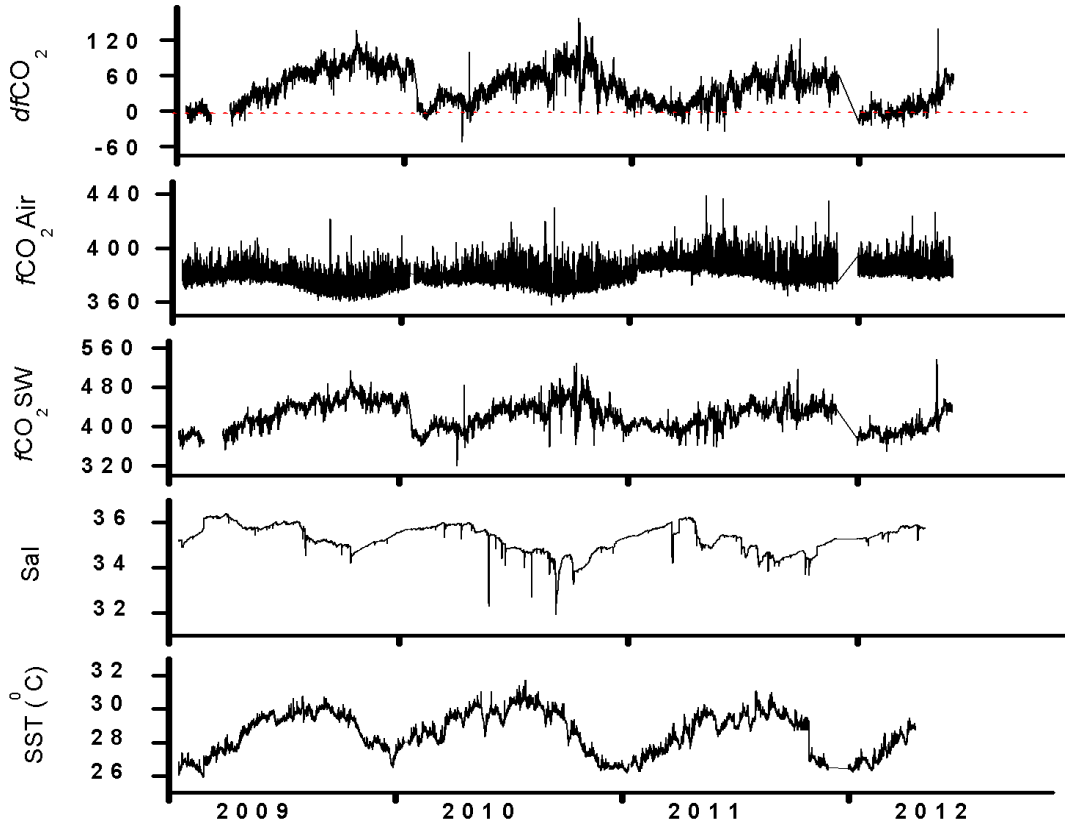

Figure 6: Multi-annual time series of sea surface temperature (^{0}C), practical salinity, air and sea in fCO_2 (μatm), and air-sea difference in fCO_2 ($dfCO_2$; μatm) at Enrique coral reef MapCO_2 buoy (n=9707).

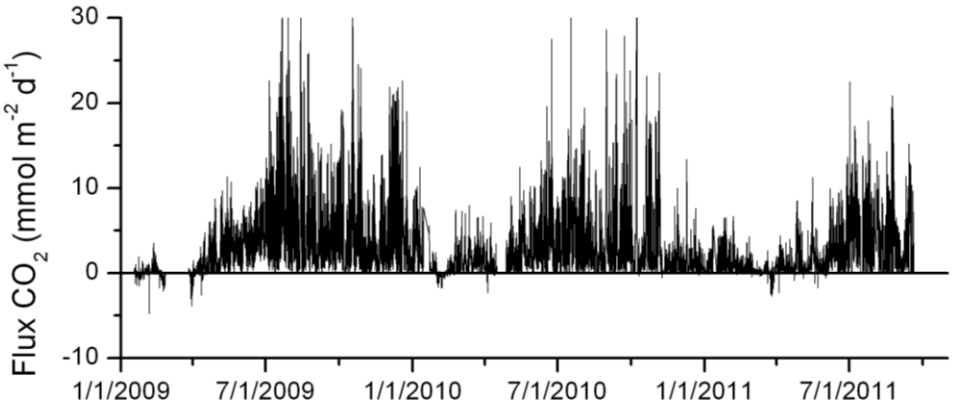

Figure 7: CO_2 flux at Enrique reef from 2009 to October 2011.

Discrete pH and TA measurements from the sample stations along La Parguera Marine Reserve (represented with orange circles in Figure 1) showed no significant difference with respect to our reef station at the MapCO_2 buoy (t-test, $p< 0.01$). The seagrass station, located at the inside part of Enrique reef, showed significant difference from the reef station and is not included in this analysis. The mean potentiometric discrete TA from 2009 to 2012 was 2291 ± 44.4 μmol kg^{-1}_{SW} (n=563). TA ranged from 2187 to 2398 μmol kg^{-1}_{SW}. TA increased during winter and spring and decreased during the summer and fall seasons. Highest and lowest TA values were observed in 2009. Total CO_2 mean was 1968 ± 35.6 μmol kg^{-1}_{SW}, ranged from 1684 to 2054 μmol kg^{-1}_{SW} (n=563). Spectrophotometric pH mean value was 8.01 ± 0.033, n=563. Maximum pH variability was of 0.23 units, from 7.86 to 8.09. Minimum values were observed in July and October 2010 and maxima in January and April 2011. Mean Ω_{arg} was 3.67 ± 0.193, n =563. Maximum Ω_{arg} variability was of 1.70 units, from 2.81 to 4.51. Minimum Ω_{arg} values were in summer and winter and maxima in spring and fall (Figure 8).

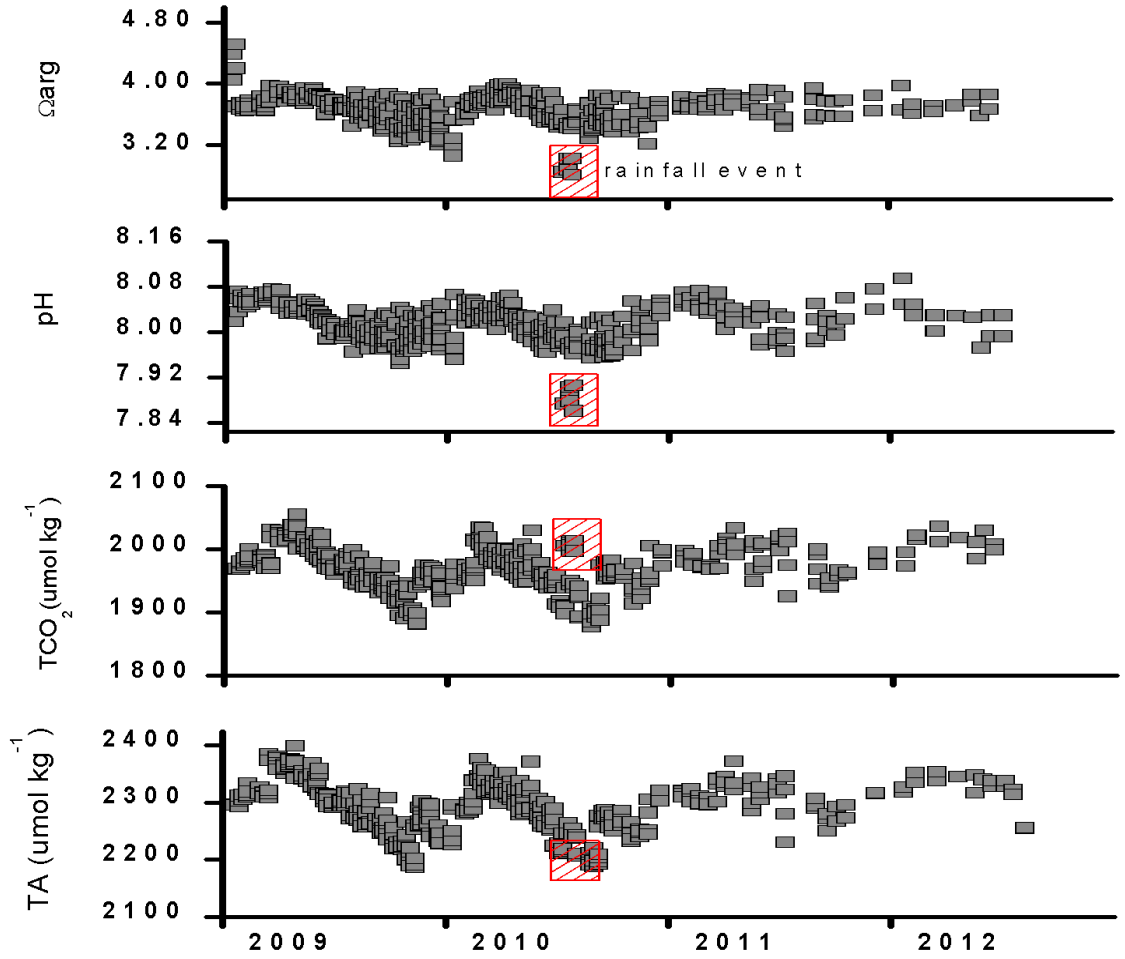

Figure 8: Time series of TA (µmol kg^{-1}_{sw}), total CO_2 (µmol kg^{-1}_{sw}), pH (total scale), and seawater carbonate saturation state (Ω) with respect to the aragonite mineral phase from discrete samples at La Parguera Marine Reserve (n=563).

1.11 Carbonate seawater difference from offshore waters and reef stations at La Parguera Marine Reserve

Significant mean differences in TA, pH, TCO_2, Ω_{arg}, and pCO_2 were observed between the offshore and the Enrique mid–shelf reef stations (t test, $p>0.05$). Table 1 summarizes the results of system parameter between the insular shelf relative to the offshore station. Mean SSS

and SST were 35.3 ± 0.5 and 28.8 ± 1.2 °C at the reef station, and 35.3 ± 0.47 and 28.5 ± 1.0 °C offshore (n=80), respectively.

Carbonate seawater difference from the offshore and reef stations are presented in Table 2. Our discrete time series carbonate chemistry measurements indicate that the maximum Ω_{arg} difference at the reef station relative to the offshore station from 2009 to 2012 was about 0.306 units. The maximum difference of CO_3^{-2} was 2.34 μmol kg^{-1}_{SW}. The maximum differences in *N*TA and *N*TCO_2 were about 66.5 and -18.1 μmol kg^{-1}_{SW}, respectively. The mean HCO_3^- ion difference is about -40.3 μmol kg^{-1}_{SW}. The TA variations can be expressed in terms of calcium ion concentration by means of equation 4. Expected maximum difference of calcium ion concentration was about 0.03 %, respectively from the offshore to the reef (Table 2)

Unlike offshore waters, where pCO_2 in air and seawater are close to equilibrium, reef waters showed a difference of up to 130 μatm. The near-reef pCO_2 increase as offshore waters are advected into the mid-shelf could be attributed to biochemical processes such as calcification and respiration. At the reef station 90% of our seawater pCO_2 measurements were observed to achieve values in excess of 385 μatm throughout the annual cycles from 2009 to 2012. Seawater pCO_2 at the reef station increases during summer and rapidly declines in winter (real-time data of air and seawater xCO_2 may be viewed at the MapCO_2 buoy site (http://www.pmel.noaa.gov/co2/story/La+Parguera).

The seawater pCO_2 measurements collected every 3 hours at the reef station show diurnal variability of 10 to 20 μatm (over a 4-day period monitoring during April 2010). This is a temporal change largely ignored in the assessment of OA on coral reefs (Dwight et al. 2008) using regional and global numerical marine carbonate system models. This gradient can be influenced by the variability in wind flow patterns and air pCO_2 associated with coastal zone

environments. The land-sea breeze has a significant effect on the reef capacity to equilibrate with atmospheric pCO_2 in tropical coastal areas, where the conditions have been observed through the whole year (Geyer, 1997; Valle-Levinson et al. 2003; Simionato et al. 2005; Hunter et al. 2007; Harrison et al. 2012).

Only one carbonate system parameter (pCO_2) showed a distinct inter-annual trend. This is seen in the pCO_2 difference between insular shelf and offshore seawater stations from 2009 to 2012. The pCO_2 difference between these two sites decreased about 0.064 μatm yr^{-1} (R^2=0.35, n=80). The other parameters showed no significant trends (Figures not shown).

Table 1: Carbonate seawater chemistry system parameters at the offshore and reef stations at La Parguera Marine Reserve from 2009 to 2012.

	Reef				Offshore			
n=80	**Mean**	**Max**	**Min**	**Range**	**Mean**	**Max**	**Min**	**Range**
SST (^{0}C)	28.8	30.5	26.4	4.14	28.5	30.4	26.4	4.04
Practical Salinity	35.3	36.2	34.1	2.09	35.3	36.0	34.1	1.98
pH	8.00	8.07	7.87	0.191	8.03	8.09	7.90	0.191
*N*TA (μmol kg^{-1}_{SW})	2262	2367	2184	183	2280	2333	2208	124
NTCO_2 (μmol kg^{-1}_{SW})	1922	2019	1828	190	1985	2070	1919	151
pCO_2 (μatm)	426	489	361	128	380	407	353	53.9
HCO^-_3 (μmol kg^{-1}_{SW})	1711	1754	1647	107	1750	1799	1720	78.8
CO^{-2}_3 (μmol kg^{-1}_{SW})	217	240	191	48.5	239	251	229	21.7
Ωarg	3.50	3.87	3.06	0.810	3.80	3.97	3.65	0.327

Table 2: Carbonate seawater differences (Δ Reef-Offshore) between the reef and offshore stations at La Parguera Marine Reserve from 2009 to 2012.

Δ Reef–Offshore (n=80)	Mean	Max	Min	Range
SST (°C)	0.356	0.976	-0.733	-1.71
Practical Salinity	0.026	0.681	-0.615	-1.30
pH	-0.029	0.077	-0.085	-0.162
*N*TA (μmol kg^{-1}_{sw})	-17.8	66.5	-75.4	-142
NTCO_2 (μmol kg^{-1}_{sw})	-63.0	-18.1	-114	-96.2
ΔTA: ΔTCO_2	0.300	1.46	-1.38	-2.84
NCa^{2+} (mol kg^{-1}_{sw})	-0.0001	0.0003	-0.0004	-0.001
pCO_2 (μatm)	46.2	110	-26.8	-137
HCO^{-}_3 (μmol kg^{-1}_{sw})	-40.3	1.78	-90.2	-92.0
CO^{-2}_3 (μmol kg^{-1}_{sw})	-22.8	2.34	-48.8	-51.1
Ωarg	-0.306	0.111	-0.760	-0.871

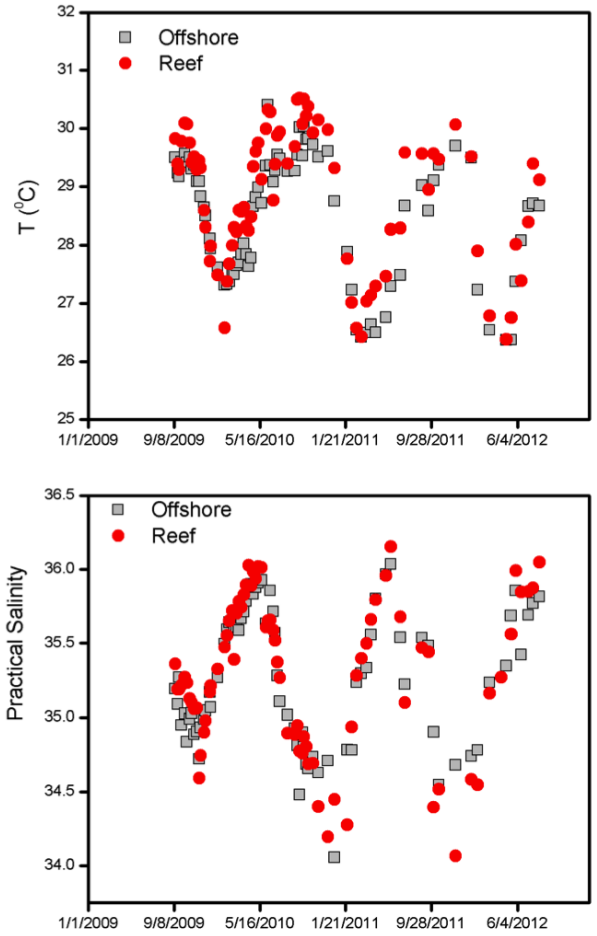

Figure 9: Discrete time series of SST (°C) and practical SSS at the offshore and reef stations from 2009 to 2012.

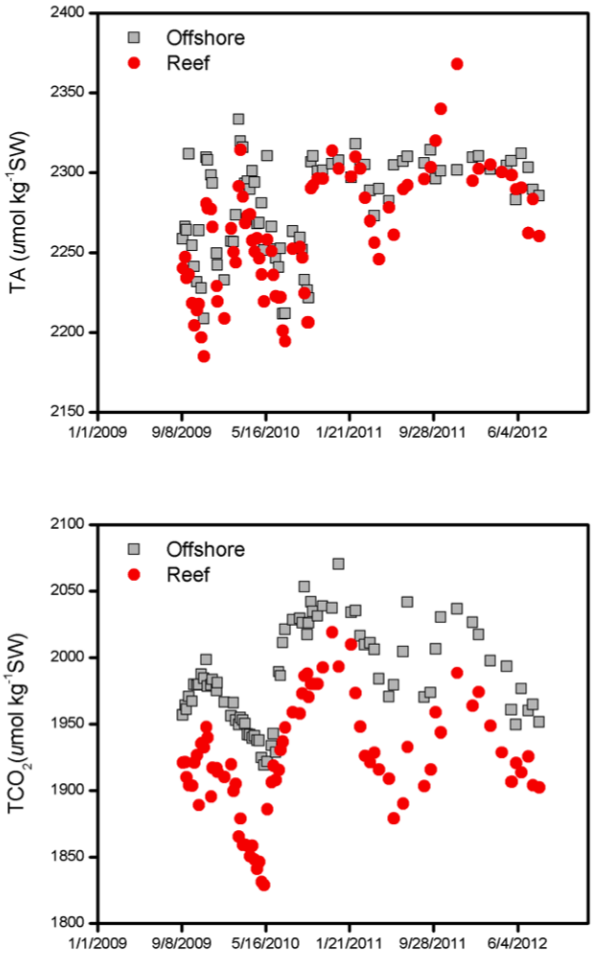

Figure 10: Discrete time series of potentiometric TA and TCO_2 (both normalized to S=35) from biweekly samples at the offshore and reef stations from 2009 to 2012.

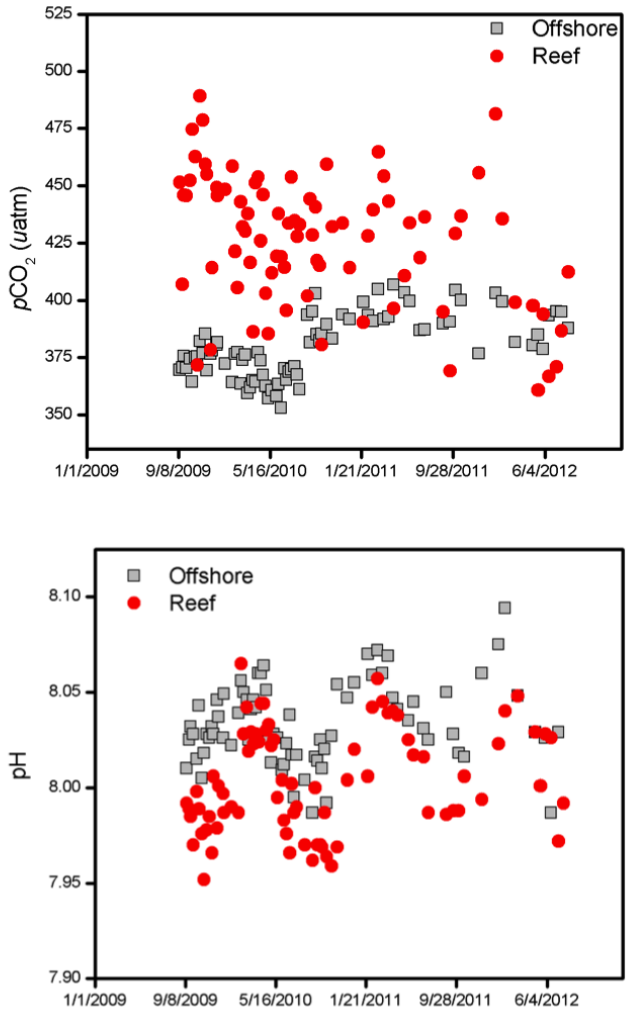

Figure 11: Time series of spectrophotometric pH (total scale) and seawater pCO_2 (μatm) at the offshore and reef stations from 2009 to 2012.

1.12 Estimation of sediment dissolution rates at Enrique forereef

Total alkalinity at Enrique Reef significantly increased with depth in the sediment column. Figure 12 shows the linear tendency for TA to increase with depth on July, June and September 2011 ($R^2 = 0.89$, $R^2 = 0.94$, $R^2 = 0.87$, respectively). This tendency showed no significant temporal variations (June through September 2011) or spatial heterogeneity. The small variations between depths can be caused by extraction and mixing of porewater from

overlying sediment layers and natural changes in the vertical diffusion of TA. The maximum *N*TA registered was 3512 µmol kg^{-1}_{SW} on September 2012 at 20 cm depth. The minimum reported was 2231 µmol kg^{-1}_{SW} at the sediment-water interface in July. The maximum *N*TA variability from the sediment-water interface was 49.7 %. The Δ*N*TA ranged from 48.8 to 75.7 µmol kg^{-1}_{SW}.

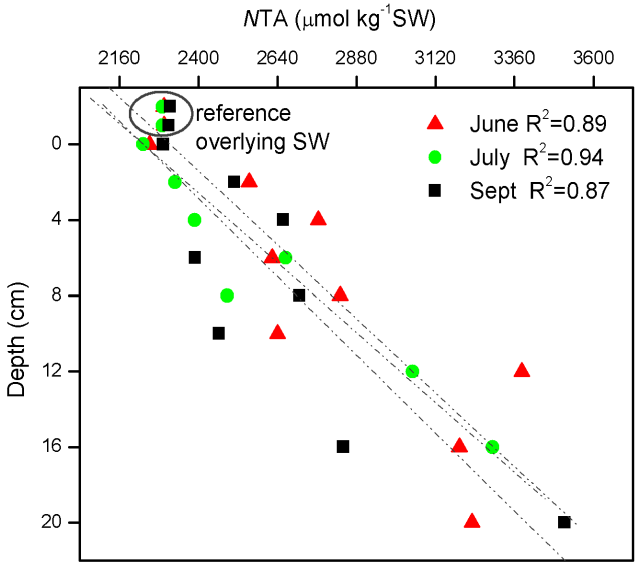

Figure 12: Sediment porewaters *N*TA (S=35) profiles of Enrique reef from June to Sept 2011. Best fits for the linear increase of *N*TA with depth are provided.

Estimation of R_{CaCO3} was based on calculation of diffusion from the sediment to the water column under an assumption of steady state. An average porosity of 0.5 from samples collected the June 12, 2011 was assumed throughout. The diffusion of TA was estimated using the HCO^-_3 coefficient of Li and Gregory (1974). The mean R_{CaCO3} thus computed was 0.003 mmol m^{-2} h^{-1}.

Porewater Ca^{2+} and Mg^{2+} concentrations increased with depth in Enrique reef sediments (Figure 3, for more details refer to Appendix 1), presumably as a result of sediment carbonate dissolution.

Table 4 presents the maximum, minimum and the variability of Mg^{2+} and Ca^{2+} sediment porewater ion concentrations from June, July and September 2011 at Enrique reef station. Maximum and minimum Ca^{2+} concentrations were 0.0132 ± 0.00003 mol kg^{-1} and 0.0095 ± 0.0001 mol kg^{-1} in June 2011. Difference of Mg^{2+} ion was about 30% greater than Ca^{2+}.

Table 3: Diffusion coefficient corrected for tortuosity (K), change in *N*TA (Δ*N*TA/Δz), total alkalinity Flux (F_{NTA}), and carbonate dissolution rates (R_{CaCO3}) for sediment porewater at Enrique Reef on June, July and September 2011.

Days	Depth (cm)	K (m^2 s^{-1})	Δ*N*TA/Δz (μmol kg^{-1} cm^{-1})	F_{NTA} (mmol m^{-2} h^{-1})	R_{CaCO3} (mmol $m^{-2}h^{-1}$)
Jun/12/11	0-20	5.90E-06	48.8	5.31E-03	0.003
July/31/11	0-20	5.90E-06	67.7	7.37E-03	0.004
Sep/09/11	0-20	5.90E-06	59.1	6.43E-03	0.003

HCO^-_3 flux from Li and Gregory (1974) = 1.18 E-05 cm^2 s^{-1}. Tortuosity correction was using the relationship between tortuosity, porosity (ϕ) and the formation resistivity factor (F) from porosity samples collected the June 12, 2011; ϕ ≈ 0.5, m = 2.

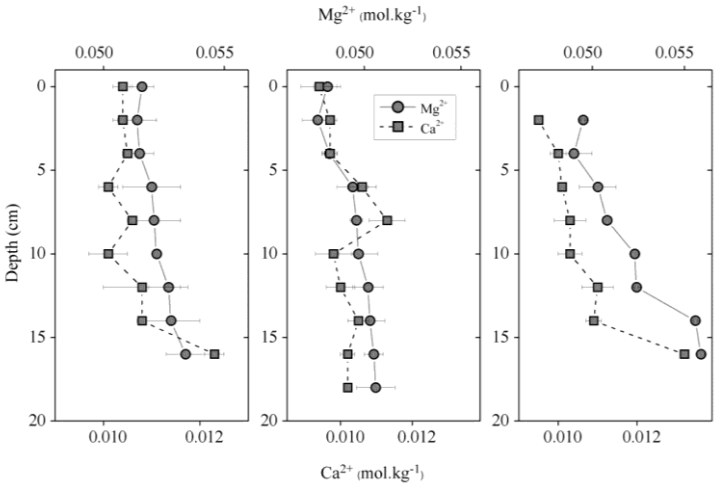

Figure 13: Vertical porewater profiles for Mg^{2+} and Ca^{2+} ion concentration at Enrique Reef June (left), July (Center), and September 2011 (right).

Table 4: Maximum, minimum and the change (%) of Mg^{2+} and Ca^{2+} sediment porewater ion concentrations from June, July, and September 2011 at Enrique reef station.

Days	[mol kg^{-1}]	Max	SD	Min	SD	Max % of Δ
Jun/12/11	Mg^{2+}	0.0559	0.0002	0.0490	0.0010	0.69
	Ca^{2+}	0.0132	0.00003	0.0095	0.0001	0.38
July/31/11	Mg^{2+}	0.0534	0.0008	0.0514	0.0008	0.19
	Ca^{2+}	0.0123	0.0002	0.0101	0.0002	0.22
Sep/09/11	Mg^{2+}	0.0506	0.0010	0.0476	0.0008	0.30
	Ca^{2+}	0.0113	0.0005	0.0097	0.0002	0.16

Discussion

1.13 Abiotic effects on La Parguera carbonate chemistry

Major climatic events have a significant effect on coastal seawater carbonate chemistry. For instance, following massive bleaching events in response to elevated SST reef community structures changes from domination by calcifying organisms to photosynthetic organisms therefore altering the local seawater carbonate chemistry. Repeated bleaching events are considered a major cause of coral mortality. In 2005, the northeastern Caribbean experienced the worse mass-bleaching event yet (Hernández-Delgado et al. 2006; Miller et al. 2009; Hernández-Pacheco et al. 2011). More than 90% of coral cover in PR and USVI was bleached causing significant loss of live tissue (Ballantine et al. 2008; Miller et al. 2009), alteration of demographic transitions of principal Caribbean reef-building corals (Hernández-Pacheco et al.

2011) and coral mass mortality (Ballantine et al. 2008). In La Parguera Marine Reserve, reduced cover of the primary reef-building corals (e.g. *Montrastea annularis and Acropora palmata*) has caused a shift of reef community structure from scleractinian to non-scleractinian domination. As a result, local seawater carbonate chemistry and other biochemical processes may be subjected to changes as well.

Bleaching events and increased susceptibility of the algal symbionts of corals to photoinhibition are associated with elevated SST (Lesser et al. 1990; Iglesias-Prieto et al. 1992; Hoegh-Guldberg & Jones, 1999). From 2009 to 2012 SST exceeded the mean monthly maximum SST for the PR-USVI area (28.5°C) at the MapCO_2 buoy reef station 56 % of the time. During the same period, the 29.5˚C threshold value for coral bleaching (according to the NOAA satellite-derived Degree Heating Week (DHW) for the Caribbean region, NOAA/NESDIS) was exceeded 32% of the time (Figure 14).

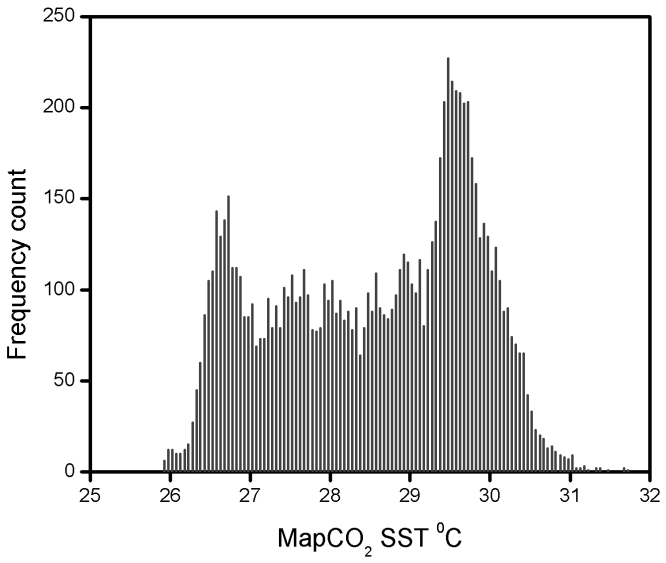

Figure 14: Seawater temperature frequency distribution at Enrique MapCO_2 buoy from 2009 to 2012 (n=9355).

Understanding and identifying the controls on surface TA and carbonate chemistry variability is becoming increasingly important for understanding the effects of ocean acidification (Feely et al. 2004; Lee et al. 2006). In La Parguera reef ecosystems, the SSS cycle is characterized by decreased salinity during the summer and fall due in large part to the influence of the Amazon and Orinoco rivers in the eastern Caribbean basin and seasonal precipitation and increased salinity during the winter and spring. Lee et al. (2006) argue that up to 80% of the variability in surface TA can be attributed to variations in SSS with a minor dependence on SST. At La Parguera reef ecosystems we find that over 60 % of the variability in TA (Figure 15) and around 39 % of the variations in pH (data not shown) are explained by changes in SSS. On the other hand, while SST shows only a weaker correlation with TA (R^2=0.33, n= 555, data not shown) it exhibits a strong negative correlation with pH (R^2= -0.74, n=555; Figure 15). The decrease in SSS and the increase in SST in the eastern Caribbean during the summer and fall may partially exacerbate ocean acidification effects by depressing surface TA and pH.

Decreases in pH, TA and therefore Ω between July and August 2010 were due principally to heavy local rainfall events between May and September 2010. The total rainfall from May to September 2010 was 862 mm, registered at the PR ICON/CREWS station. The San Juan, PR Weather Forecast Office July 2010 climate report identified this month as well above normal in terms of precipitation (illustrate at Figure 8 as a rainfall event). At the Luis Muñoz Marin International Airport in San Juan, the monthly precipitation was about 110 mm above normal. TA showed positive correlation with pH (R^2= 0.68) and TCO_2 (R^2= 0.95) and some negative correlation with pCO_2 (R^2= -0.52) (Figure 16). The positive correlation between TA and TCO_2 and pH and the inverse correlation with pCO_2 suggests that photosynthesis and biogenic

precipitation of calcium carbonate are also the major processes affecting La Parguera carbonate chemistry.

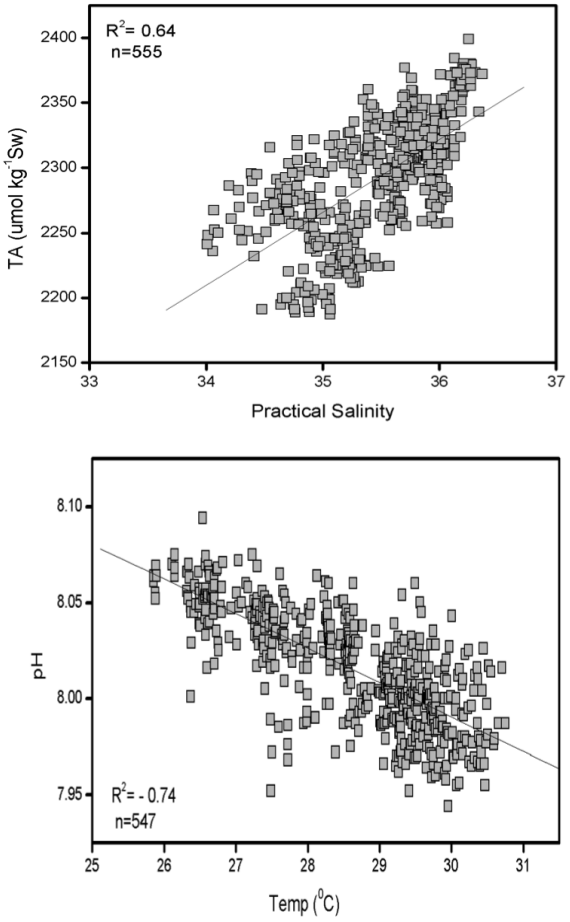

Figure 15: Linear correlations between SSS and TA, and SST and pH at La Parguera Marine Reserve.

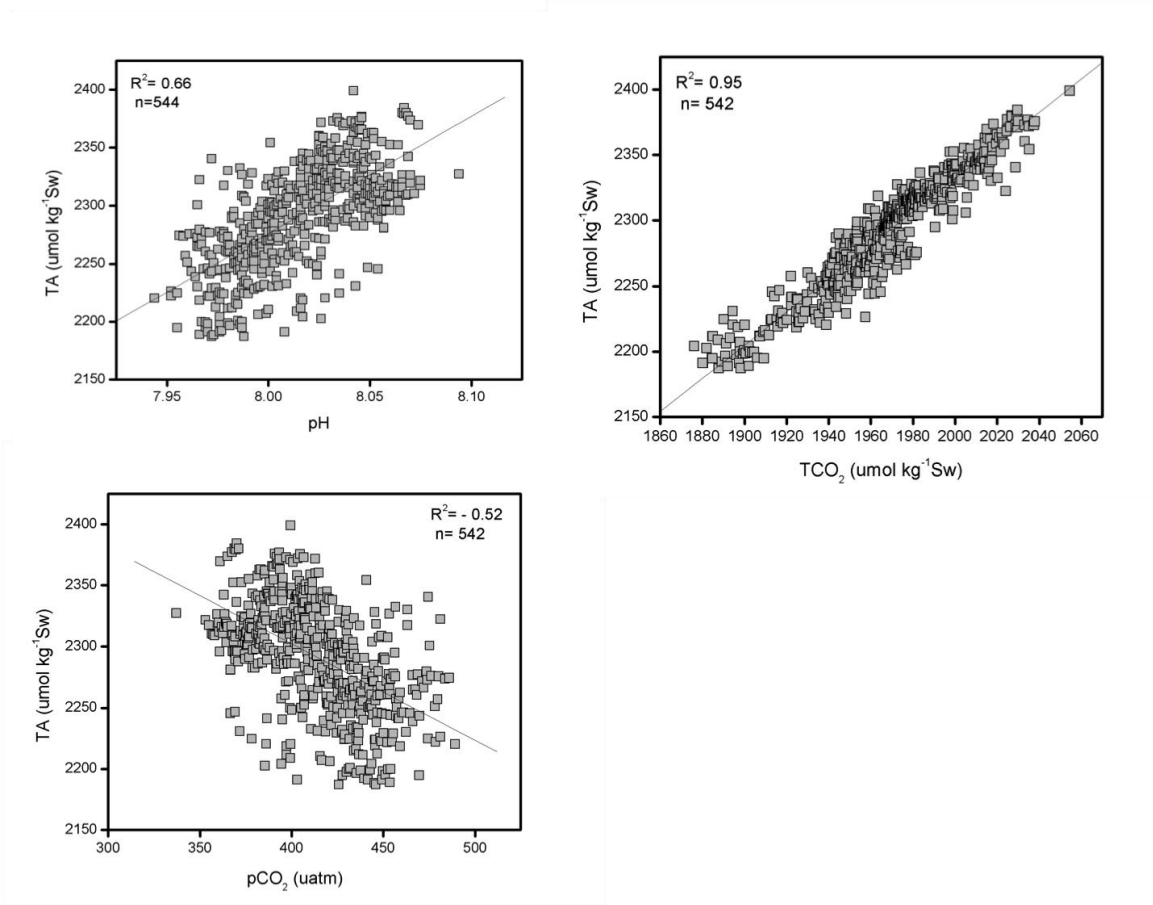

Figure 16: Linear correlations of pH, TCO_2 and pCO_2 with TA at La Parguera Marine Reserve from 2009 to 2012.

Different near-reef hydrodynamic conditions (currents and water-level variation from tides) can alter TA and TCO_2. Water mixing of TCO_2 from tidal flooding of the nearby mangrove, seagrasses, and sandy lagoons wetland areas of La Parguera can significantly contribute to the local and seasonal variability of TCO_2. There is evidence that during lunar perigees and apogees, La Parguera coastal ecosystems have experience seiches with periods of 50 minutes (Sosa, 2012). These events occur twice a year and differ in intensity, duration and dates every year. Additional examination is required to assess the effect of these events on carbonate chemistry variations at La Parguera.

1.14 Evidence of $CaCO_3$ calcification at Enrique Mid-shelf reef relative to offshore water

Gattuso et al. (1999) characterized the effect of coral community metabolism on the seawater carbonate system using the ratio of change in the buffer capacity (ΔTA) to the change in acidity (ΔTCO_2). They note that this ratio ($\Delta TA/\Delta TCO_2$) depends on the relative rates of calcification and photosynthesis such that $\Delta TA/\Delta TCO_2$ can range from 0 to 2.The ratio approaches 2 when calcification is active and photosynthesis is minimal, and approaches 0 when only net photosynthesis occurs. Figure 17 shows a schematic representation by Zeebe and Wolf-Gladrow (2001) of the mayor processes affected by changes on TA and TCO_2. The ΔNTA-$\Delta NTCO_2$ diagram illustrates how these carbonate parameters are each altered by processes of calcification, dissolution, respiration, and photosynthesis. In coral reef environments, where calcification is dominant (but not the only) process affecting seawater chemistry, $\Delta TA/\Delta TCO_2$ is near 0.5 (Gattuso et al. 1999).

For Enrique reef relative to the offshore station we observed a mean $\Delta TA/\Delta TCO_2$ ratio of 0.300 over the observation period. During the months of summer and fall we found that the ratio was greatest. During the period of September through October of 2011 an apparent increase in TA favored photosynthetic processes at the reef relative to the offshore station. Observations at La Parguera indicate that calcium carbonate precipitation and photosynthesis dominate throughout the year at Enrique reef (Figure 18).

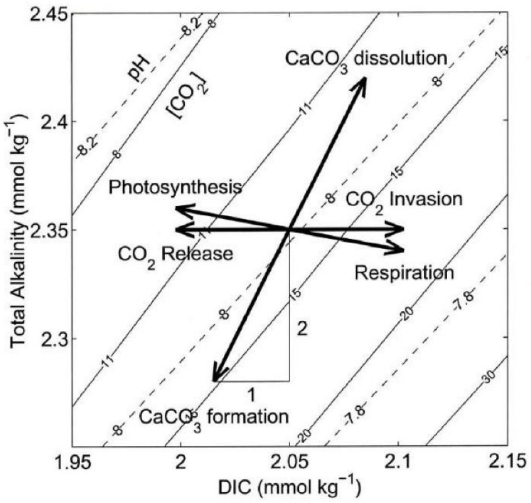

Figure 17: Schematic illustration of the effect of different biological processes on DIC and TA concentration. Contour dashed lines represent constant pH values and solid lines constant CO_2 (µmol kg^{-1}). During calcification processes DIC and TA concentration decrease by 1:2 units. Figure from Zeebe and Wolf-Gladrow (2001).

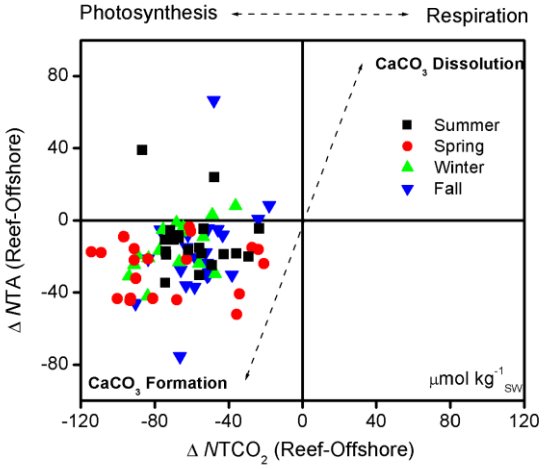

Figure 18: Differences in TA and TCO_2 concentration (normalized to S=35) between Enrique reef and offshore stations (n=80, mean $\Delta TA/\Delta TCO_2 = 0.300 \pm 0.353$) illustrating the different processes that affect TA and TCO_2 at the reef station relative to offshore waters.

Although the seawater carbonate saturation state remains supersaturated ($\Omega > 1$) with respect to the aragonite mineral phase at La Parguera, we repeatedly observed "low" values during the fall season at the reef station. Guinotte et al. (2003) and others define various

carbonate saturation state levels as regards to their capacity to support calcification by reef corals as thresholds values. Marine surface waters with a $\Omega_{arg} > 4$ are categorized as "optimal", values from 3.5 to 4 are considered "adequate", values from 3 to 3.5 are "low", and those below 3 are deemed ''extremely marginal''. The degree of aragonite saturation is currently decreasing across the Caribbean Region at a rate of about 3% per decade and exhibits considerable spatial and seasonal variability (Gledhill et al. 2008). Significant differences are found between the near-reef Ω_{arg} and offshore values (t-test, $p<0.0001$, SE= 0.020). Offshore waters show Ω_{arg} mean values of 3.80, whereas reef station can reach values as low as 3.06. Difference in carbonate saturation state within the near-reef environment is distinct from those observed in surface offshore waters by 31 % (Table 2). Change from the offshore Ω_{arg} values is in large part attributable to active calcification on the reef during the period of sampling. Other environmental variables such as local rainfall, coastal river runoff, calcification, and dissolution processes can significantly depress Ω_{arg} in coastal environments and they may not be so apparent in offshore waters (Figure 19).

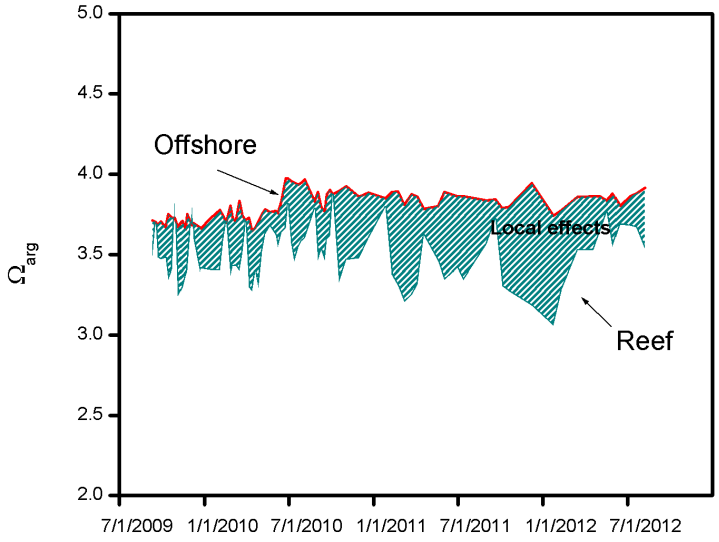

Figure 19: Time series of Ω_{arg} at Enrique reef station (green line) compared to the offshore station (red line). During the summer and fall, reef values decrease considerably due to the "local effects" (hatched green area).

While estimation of net calcification rates is impossible without reliable estimates of water mass residence times over the shelf-edge at La Parguera, these data are indicative of vigorous calcification. Based on observed changes in porewater TA and estimates of vertical flux of TA in sediment porewaters, preliminary data on carbonate dissolution is estimated as 0.003 mmol m^{-2} h^{-1} in the summer of 2011 at Enrique forereef. Using an estimated area of Enrique reef of 0.57 km^2, on an annual basis, this corresponds to 3.04 g $CaCO_3$ m^{-2} $year^{-1}$. A weekly 2009 data set of Eulerian estimates (Langdon personal communication) indicates an annual gross calcification rate at Enrique coral reef of 825 g $CaCO_3$ m^{-2} $year^{-1}$ (unpublished data), which is a significant fraction of the present day estimate of the average global coral reef calcification of 1,500 g $CaCO_3$ m^{-2} $year^{-1}$ (Andersson et al. 2007).

Due to the small value of estimated dissolution rate using vertical flux of TA (see below), there is no apparent significant difference between gross and net calcification rates at Enrique

reef during the time of study. More information would be necessary to estimate the tipping point between gross calcification and dissolution rate.

1.15 Estimation of sediment dissolution rates

Sediment TA profiles reflect carbonate mineral dissolution with increased TA, Ca^{2+} and Mg^{2+} porewater content. Thermodynamically, the saturation state is strongly correlated with the rate of formation or dissolution of the carbonate minerals. In this study we did not test for pH making estimation of the saturation state difficult. However, the TA differences show that the sediment Ω_{arg} at Enrique reef decreases as a function of depth, suggesting that the rate of formation of aragonite mineral decreases as depth increases. In estimating calcium carbonate dissolution rates in carbonate porewaters in accordance with Fick's First Law (eq. 8) we found extremely low dissolution rates for carbonate sediments and coral reef areas (Table 5), about 2 orders of magnitude of under the assumption of molecular diffusion alone. However, shelf areas and permeable sediments display conditions that do not allow assumptions of steady state. Here advective processes can occur, as for example the permeability of sandy sediments, the topography, and the presence of oscillating currents (Precht & Huettel, 2004; Cook et al. 2007). Enrique forereef is a dynamic area where energetic sediment-transport can be taking place especially during the times of long period waves. In this context further information is necessary to calculate the permeability of Enrique sediments. Porewater mixing and transport can be dominated by wave-induced mechanisms and bottom currents and should not be overlooked. Vertical diffusivity fluxes using fluorometric technique could improve the estimation of dissolution rates at Enrique reef sediments. Jahnke et al. (2005) noted that for sediments with permeabilities > ~ 10-12 cm^2 (fine sand and coarser; ~100 mm median grain size), advection and

enhanced dispersion may dominate porewater transport (Huettel & Webster, 2001; Reimers et al. 2004).

Table 5: Different carbonate dissolution rates for carbonate environments. Modified from Andersson et al. (2007).

Environment	Dissolution rates (mmol m^{-2} h^{-1})	References
Enrique coral sediments	0.003	This study*
Carbonate sediments	0.2-0.8	Andersson et al. (2007)
Patch reef 22% coral cover	0.3-3.0	Yates & Halley (2006)
Patch reef 10% coral cover	0.1-0.5	Yates & Halley (2006)
Coral rubble	0.2-2.0	Yates & Halley (2006)
Sand bottom	0.05-0.6	Yates & Halley (2006)
Seagrass	0.4	Yates & Halley (2003)
Sand bottom	0.3	Yates & Halley (2003)
Patch reef 10% coral cover	0.5	Yates & Halley (2003)
Sand community	0.8	Leclercq et al. (2002)
High Mg-calcite sediments	0.2	Langdon et al. (2000)
Sandy bottom reef flat and lagoon	0.8	Boucher et al. (1998)
Carbonate sediments	0.3	Balzer & Wefer (1981)

* Estimation based on porosity of 0.5 from samples collected from June to September 2011. The diffusion coefficient of TA was estimated using the HCO_3 flux from Li and Gregory (1974).

Porewater Ca^{2+} and Mg^{2+} measurements provide additional evidence for the occurrence of sediment carbonate dissolution and the preferential dissolution of high-Mg calcite (Mackenzie et al. 1983; Burdige & Zimmerman, 2002; Morse et al. 2006). Presumably due to the content of biogenic high Mg-calcites (>3-4mol% $MgCO_3$) in these sediments that exceed the solubility of aragonite at ~12mol% $MgCO_3$ (Reader, 1983; Mackenzie et al. 1983; Bischoff et al.1983; Morse et al. 2006). Figure 20 and Figure 21 show linear regressions between Ca^{2+} and Mg^{2+} sediment porewater ion concentrations and *N*TA at Enrique area. Positive correlation between Ca^{2+} and *N*TA is observed in June (R^2= 0.73, n=8, p=0.04) and July (R^2= 0.81, n=6, p=0.05). No significant correlation between these two parameters was observed in September. Stronger positive linear correlation between Mg^{2+} and *N*TA is observed in June (R^2= 0.73, n=8, p= 0.04)

and July (R^2= 0.96, n=6, *p*= 0.002), and September (R^2= 0.57, n=7, *p*= 0.1). Morse and Mackenzie (1990) noted that high-Mg skeletal calcite could have up to 30 mol% Mg. Burdige and Zimmerman (2002) show that the dissolution of 20 mol% Mg-calcite would decrease the $\Delta Ca^{2+}/\Delta TA$ ratio from 0.5 to 0.4 or even lower if the calcium ions are precipitated by carbonate minerals.

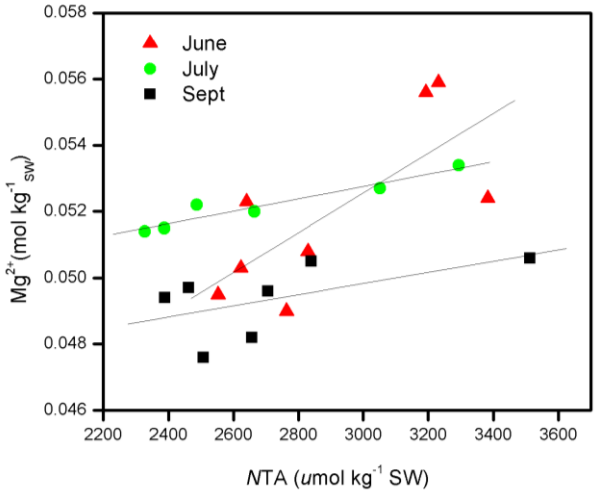

Figure 20: A plot of sediment porewater Mg^{2+} concentration against *N*TA.

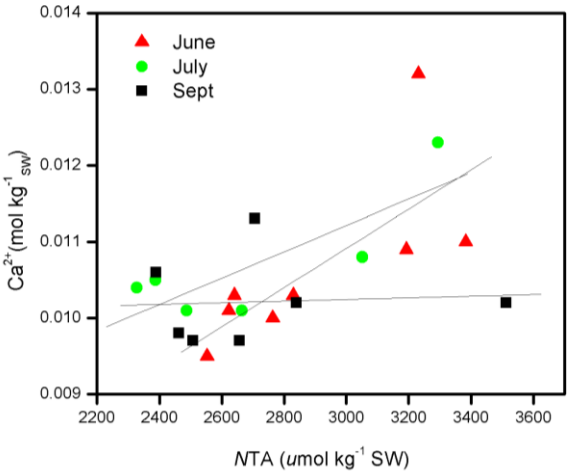

Figure 21: A plot of sediment porewater Ca^{2+} concentration against *N*TA.

Conclusions

The first three objectives were related to the development of a method to determine both Ca^{2+} and Mg^{2+} concentrations in seawater and sediment porewaters and to determine the precision of Ca^{2+} measurements necessary to discern changes by shelf calcifiers at La Parguera. After testing various IAPSO Standard Seawater, porewater and surface seawater samples in various different analytical conditions, we can conclude that:

1) The method explained in Appendix 1 resulted in a better method for rapid quantification of seawater Ca^{2+} and Mg^{2+} alkaline earth metals compared with other gravimetric procedures and titration methods.
2) No significant difference between reef and offshore water samples was observed. The relatively low changes between surface seawater concentrations of Ca^{2+} and Mg^{2+} cations at surface near-reef environments make this method, as tested, unsuitable to determine changes due to biotic or abiotic calcification. However, the precision achieved using the HPCIC system is applicable to study the large variations of Mg^{2+} and Ca^{2+} ions observed in marine sediment porewaters.
3) Further developments in methodology and instrumentation are required in order to better estimate small changes in seawater. An immediate objective should be testing of large bore monolithic columns with higher carrying capacity.
4) Observations of alkalinity changes indicate that calcification in this coral reef environment can be expected to change the Ca^{2+} concentration by less than ~ 0.03 % over a year cycle. This confirms the need for high precision and the challenges to Ca^{2+} and Mg^{2+} measurements in surface seawater.

The fourth objective was estimating carbonate mineral dissolution rates in the sediment porewaters. To this end we conclude:

1) The mean R_{CaCO3} thus computed was 0.003 mmol m-^{2} h^{-1} and average vertical flux of TA at Enrique sediment porewater was 0.006 mmol m^{-2} h^{-1}.
2) Extremely low dissolution rates, for carbonate sediments and coral reef areas, on order of magnitude of about ~ 2 units below published estimates for similar environments under the assumption of molecular diffusion alone. Accordingly, permeability to advective processes at Enrique reef should be taken it in account.
3) TA gradient fluxes will give us a good estimation of the predominant processes at the reef (calcification or dissolution) and the carbonate mineral phase composition of the boundary layer.
4) Sediment TA profiles suggest little temporal variability in sediment porewater TA concentration.

Our last objective was characterizing seasonality of the carbonate system at La Parguera. To this end we conclude:

1) Changes in pH and TA at La Parguera are strongly associated with variability in SST and SSS. TA showed strong correlation with variations in TCO_2.
2) During the summer the SST at the Reef station can exceed the 30˚C threshold value for coral bleaching. SSS decrease during the summer due to the influx of the Orinoco plume into the eastern Caribbean basin and seasonal local precipitation.
3) Future precipitation changes due to climate change may have a significant effect on TA in the NE Caribbean.

4) The decrease in carbonate concentration results in a decrease in carbonate saturation state. Maxima and minima are in April and September, respectively for carbonate concentration and carbonate saturation state. Although the Ω_{arg} remains supersaturated, we observed seasonal depression during the fall at the Reef station.
5) Calcification and photosynthesis are the major process controlling carbonate chemistry at Enrique reef. Differences in TA and TCO_2 concentration between Enrique reef and offshore stations showed no significant seasonal variations throughout the observation period (2009 - 2012).
6) These datasets should continue in order to reproduce seasonal dynamics, to assess inter-annual variability and to detect long-term trends on near-reef coastal environments at La Parguera Marine Reserve.
7) The discrete measurements helped validate and supplement the $MapCO_2$ buoy observations. These efforts will establish a critical baseline against which future comparisons can be made to evaluate ocean acidification impacts, including the potential risk of reef framework degradation.

References

Andersson, A.J., Bates, N.R., & Mackenzie, F.T. (2007). Dissolution of Carbonate Sediments Under Rising pCO_2 and Ocean Acidification: Observations from Devil's Hole, Bermuda. *Aquatic Geochemistry*, *13*(3): 237–264. doi:10.1007/s10498-007-9018-8.

Andersson, A.J., Mackenzie, F.T., & Bates, N.R. (2008). Life on the margin: implications of ocean acidification on Mg-calcite, high latitude and cold-water marine calcifiers. *Marine Ecology Progress Series*, *373*: 265–273. doi:10.3354/meps07639.

Andersson, A.J., Mackenzie, F.T., & Lerman, A. (2005). Coastal ocean and carbonate systems in the high CO_2 world of the Anthropocene. *American Journal of Science*, 305: 875–918.

Andersson, A.J., Mackenzie, F.T., & Ver, L.M. (2003). Solution of shallow-water carbonates: An insignificant buffer against rising atmospheric CO_2. *Geology*, *31*(6): 513. doi:10.1130/0091-7613(2003)031<0513:SOSCAI>2.0.CO;2.

Archie, G.E. (1942). The electrical resistivity log as an aid in determining some reservoir characteristics. *Transactions of the American Institute of Mining and Metallurgical Engineers*, 146: 54–62.

Artioli, Y., Blackford, J.C., Butenschön, M., Holt, J.T., Wakelin, S.L., Thomas, H., Borges, A. V., et al. (2012). The carbonate system in the North Sea: Sensitivity and model validation. *Journal of Marine Systems*, *102-104*:1–13.doi:10.1016/j.jmarsys.2012.04.006.

Atkinson, M.J. & Cuet, P. (2008). Possible effects of ocean acidification on coral reef biogeochemistry: topics for research. *Marine Ecology Progress Series*, 373: 249-256.

Ballantine, D. L., et al. (2008). Biology and ecology of Puerto Rican coral reefs. Pages 375–406. in M. B. Riegl and R. E. Dodge, editors. Coral reefs of the USA. Springer-Science.

Balzer, W., & Wefer, G. (1981) Dissolution of carbonate minerals in a subtropical shallow marine environment. *Marine Chemistry*, 10: 545–558.

Basterretxea, G., Jordi, A., Garcés, E., Anglès, S., & Reñé, A. (2011). Seiches stimulate transient biogeochemical changes in a microtidal coastal ecosystem. *Marine Ecology Progress Series*, *423*: 15–28. doi:10.3354/meps08949.

Bates, N.R., Samuels, L., & Merlivat, L. (2001). Biogeochemical and physical factors influencing seawater fCO_2 and air-sea CO_2 exchange on the Bermuda coral reef. *Limnology and Oceanography*, 46(4):833–846. doi:10.4319/lo.2001.46.4.0833.

Berner, R.A. (1980). Early diagenesis: A theoretical approach (No. 1). Princeton University Press.

Berner, R.A. (2004). A model for calcium, magnesium and sulfate in seawater over Phanerozoic time. *American Journal of Science*, *304*(5):438–453. doi:10.2475/ajs.304.5.438.

Bischoff, W.D., Bishop, F.C., Mackenzie, F.T. (1983). Biogenically produced magnesian calcite: inhomogeneities in chemical and physical properties; comparison with synthetic phases. *American Mineralogist*, 68:1183–1188.

Boucher, G., Clavier, J., Hily, C., & Gattuso, J.P. (1998). Contribution of soft-bottoms to the community metabolism (primary production and calcification) of a barrier reef flat (Moorea, French Polynesia). *Journal of Experimental Marine Biology and Ecology*, *225*(2): 269-283.

Burdige, D.J., & Zimmerman, R.C. (2002). Impact of sea grass density on carbonate dissolution in Bahamian sediments. *Limnology and Oceanography*, *47*(6):1751–1763.

Burdige, D.J., Zimmerman, R.C., & Hu, X. (2008). Rates of carbonate dissolution in permeable sediments estimated from pore-water profiles: The role of sea grasses. *Limnology and Oceanography*, *53*(2): 549–565. doi:10.4319/lo.2008.53.2.0549.

Caldeira, K., & Berner, R. (1999). Seawater pH and Atmospheric Carbon Dioxide. *Science*, *286*(5447): 2043. doi:10.1126/science.286.5447.2043a.

Caldeira, K., & Wickett, M.E. (2003). Oceanography: anthropogenic carbon and ocean pH. *Nature*, *425*(6956): 365.

Climate Report for Puerto Rico and the U.S. Virgin Islands. (2010, July).*Climate Reports*. Retrieved April 10, 2013, from http://www.srh.noaa.gov/sju/?n=jul2010cr.

Cook, P.L., Wenzhöfer, F., Glud, R.N., Janssen, F., & Huettel, M. (2007). Benthic solute exchange and carbon mineralization in two shallow subtidal sandy sediments: Effect of advective pore-water exchange. *Limnology and Oceanography, 52*(5):1943-1963.

Corredor, J.E., & Morell, J.M. (2001). Seasonal variation of physical and biogeochemical features in eastern Caribbean Surface Water. *Journal of Geophysical Research*, *106*(C3): 4517–4525. doi:10.1029/2000JC000291.

Cullison, S.E. (2010). *Marine Applications of an Autonomous Indicator-based Ph Sensor* (Doctoral dissertation, The University of Montana).

Dickson, A.G. (1990). Thermodynamics of the dissociation of boric acid in synthetic seawater from 273.15 to 318.15 K. *Deep Sea Research Part A. Oceanographic Research Papers*, *37*(5): 755-766.

Dickson, A.G., & Millero, F.J. (1987). A comparison of the equilibrium constants for the dissociation of carbonic acid in seawater media. *Deep Sea Research Part A. Oceanographic Research Papers, 34*(10): 1733-1743.

Dickson, A.G., Afghan, J.D., & Anderson, G.C. (2003). Reference materials for oceanic CO_2 analysis: a method for the certification of total alkalinity. *Marine Chemistry*, *80*(2): 185-197.

Dickson, A.G., Goyet, C., & Kozyr, A. (2007). Guide to best practices for ocean CO_2 measurements. (A. J. R. C. Andrew G. Dickson, Christopher L. Sabine, Ed.) *Analysis*. PICES Special Publication.

Dlugokencky, E & Tans, P. *Trends in Atmospheric Carbon Dioxide.* Available: http://www.esrl.noaa.gov/gmd/ccgg/trends/. NOAA/ESRL, Last accessed 4th May 2013.

DOE (1994) Handbook of methods for the analysis of the various parameters of the carbon dioxide system in seawater; version 2 Dickson AG and Goyet C (eds) ORNL/CDIAC-74.

Enos, P., & Sawatsky, L.H. (1981). Pore networks in Holocene carbonate sediments. *Journal of Sedimentary Research*, *51*(3).

Falter, J.L., & Sansone, F.J. (2000). Hydraulic control of pore water geochemistry within the oxic-suboxic zone of a permeable sediment. *Limnology and Oceanography*, *45*(3): 550–557. doi:10.4319/lo.2000.45.3.0550.

Falter, J.L., Atkinson, M.J., & Coimbra, C.F.M. (2005). Effects of surface roughness and oscillatory flow on dissolution of plaster forms: evidence for nutrient mass transfer to coral reef communities. *Limnology and Oceanography, 50*: 246–254.

Falter, J.L., Atkinson, M.J., Lowe, R.J., Monismith, S.G., & Koseff, J.R. (2007). Effects of nonlocal turbulence on the mass transfer of dissolved species to reef corals. *Limnology and Oceanography, 52*: 274–285.

Feely, R.A., Sabine, C.L., Lee, K., Berelson, W., Kleypas, J.A., Fabry, V.J., & Millero, F.J. (2004). Impact of anthropogenic CO_2 on the $CaCO_3$ system in the oceans. *Science, 305*(5682): 362–6. doi:10.1126/science.1097329.

Froelich, P.N., Klinkhammer, G.P., Bender, M.A.A., Luedtke, N.A., Heath, G.R., Cullen, D., ... & Maynard, V. (1979). Early oxidation of organic matter in pelagic sediments of the eastern equatorial Atlantic: suboxic diagenesis. *Geochimica et Cosmochimica Acta, 43*(7): 1075-1090.

Gattuso, J.P., Allemand, D., & Frankignoulle, M. (1999). Photosynthesis and Calcification at Cellular, Organismal and Community Levels in Coral Reefs: A Review on Interactions and Control by Carbonate Chemistry. *Integrative and Comparative Biology, 39*(1): 160–183. doi:10.1093/icb/39.1.160.

Gledhill, D.K., Wanninkhof, R., Millero, F.J., & Eakin, M. (2008). Ocean acidification of the Greater Caribbean Region 1996–2006. *Journal of Geophysical Research, 113*(C10031): 1–11. doi:10.1029/2007JC004629.

Global Carbon Project (2008, September 26) Carbon budget and trends 2007. Retrieved May 2009, from Global Carbon Project : www.globalcarbonproject.org

Guinotte, J.M., & Fabry, V.J. (2008). Ocean acidification and its potential effects on marine ecosystems. *Annals of the New York Academy of Sciences, 1134*: 320–42. doi:10.1196/annals.1439.013.

Guinotte, J.M., Buddemeier, R.W., & Kleypas, J.A. (2003). Future coral reef habitat marginality: temporal and spatial effects of climate change in the Pacific basin. *Coral Reefs, 22*(4): 551-558.

Hernández-Delgado, E.A., Toledo, C., Claudio, H.J., Lassus, J., Lucking, M.A., Fonseca, J., Hall, K., Rafols, J., Horta, H., & Sabat, A.M. (2006). Spatial and taxonomic patterns of coral bleaching and mortality in Puerto Rico during year 2005. Satellite Tools and Bleaching Response Workshop: Puerto Rico and the Virgin Islands. St. Croix, U.S. Virgin Islands. 16 pp.

Hernández-Pacheco, R., Hernández-Delgado, E.A., & Sabat, A.M. (2011). Demographics of bleaching in a major Caribbean reef-building coral: Montastraea annularis. *Ecosphere, 2*(1): art9. doi:10.1890/ES10-00065.1.

Hoegh-Guldberg, O., & Jones, R.J. (1999). Photoinhibition and photoprotection in symbiotic dinoflagellates from reef-building corals. *Marine Ecology Progress Series, 183*: 73-86.

Hönisch, B., Ridgwell, A., Schmidt, D. N., Thomas, E., Gibbs, S. J., Sluijs, A., Zeebe, R., et al. (2012). The Geological Record of Ocean Acidification. *Science, 335*(6072): 1058–1063. doi:10.1126/science.1208277.

Hubbard, D.K., Burke, R.B., Gill, I.P., Ramirez, W.R., & Sherman, C. (2008). Coral-reef geology: Puerto Rico and the US Virgin Islands. In *Coral Reefs of the USA* (pp. 263-302). Springer Netherlands.

Huettel, M., & Webster, I.T. (2001). Porewater flow in permeable sediments. *The benthic boundary layer: transport processes and biogeochemistry. Oxford University Press, New York*, 144-179.

Iglesias-Prieto, R., Matta, J.L., Robins, W.A., & Trench, R.K. (1992). Photosynthetic response to elevated temperature in the symbiotic dinoflagellate Symbiodinium microadriaticum in culture. *Proceedings of the national Academy of Sciences, 89*(21): 10302-10305.

IPCC (2001) The Third Assessment Report of the Intergovernmental Panel on Climate Change (IPCC). Cambridge University Press: Cambridge, UK and New York, USA.

IPCC (2007) Fourth Assessment Report of the Intergovernmental Panel on Climate Change (IPCC). Valencia, Spain.

Irving, L. (1926). The Precipitation of Calcium and Magnesium from Sea Water. *Journal of the Marine Biological Association of the United Kingdom*, *14*(02): 441–446. doi:10.1017/S002531540000792X.

IUCN and UNEP-WCMC. (2009). The World Database on Protected Areas (WDPA) [http://www.wdpa.org/]. Cambridge, UK: UNEP-WCMC. Retrieved May 06, 2012 available at:www.protectedplanet.net.

Jahnke, R., Richards, M., Nelson, J., Robertson, C., Rao, A., & Jahnke, D. (2005). Organic matter remineralization and porewater exchange rates in permeable South Atlantic Bight continental shelf sediments. *Continental Shelf Research*, *25*(12-13): 1433–1452. doi:10.1016/j.csr.2005.04.002.

Kanamori, S., & Ikegami, H. (1980). Computer-processed potentiometric titration for the determination of calcium and magnesium in sea water. *Journal of the Oceanographical Society of Japan*, *36*(4): 177–184. doi:10.1007/BF02070330.

Kleypas, J.A., Buddemeier, R.W., Archer, D., Gattuso, J.P., Langdon, C., & Opdyke, B.N. (1999). Geochemical consequences of increased atmospheric carbon dioxide on coral reefs. *Science*, *284*(5411): 118-120.

Kleypas, J.A., Feely, R.A., Fabry, V.J., Langdon, C., Sabine, C.L., & Robbins, L.L. (2006). Impacts of Ocean Acidification on Coral Reefs and Other Marine Calcifiers: A Guide for Future Research, report of a workshop held 18–20 April 2005, St. Petersburg, FL, sponsored by NSF, NOAA, and the U.S. Geological Survey. 88.

Koczy, F.F. (1956). The specific alkalinity. *Deep Sea Research (1953)*, *3*(4): 279–288. doi:http://dx.doi.org/10.1016/0146-6313(56)90018-1.

Langdon, C., Broecker, W.S., Hammond, D.E., Glenn, E., Fitzsimmons, K., Nelson, S.G., ... & Bonani, G. (2003). Effect of elevated CO_2 on the community metabolism of an experimental coral reef. *Global Biogeochemical Cycles*, *17*(1).

Langdon, C., Takahashi, T., Sweeney, C., Chipman, D., Goddard, J., Marubini, F., ... & Atkinson, M.J. (2000). Effect of calcium carbonate saturation state on the calcification rate of an experimental coral reef. *Global Biogeochemical Cycles*, *14*(2): 639-654.

Le Quéré, C., Raupach, M.R., Canadell, J.G., & Marland, G. (2009). Trends in the sources and sinks of carbon dioxide. *Nature Geoscience*, *2*(12): 831-836.doi:10.1038/ngeo689.

Leclercq, N., Gattuso, J.P., & Jaubert, J. (2002). Primary production, respiration, and calcification of a coral reef mesocosm under increased CO_2 partial pressure. *Limnology and Oceanography*, *47*(2): 558-564.

Lee, K., Tong, L. T., Millero, F. J., Sabine, C. L., Dickson, A. G., Goyet, C., ... & Key, R. M. (2006). Global relationships of total alkalinity with salinity and temperature in surface waters of the world's oceans. *Geophysical Research Letters*, *33*(19): 1–5. doi:10.1029/2006GL027207.

Lesser, M.P., Stochaj, W.R., Tapley, D.W., & Shick, J.M. (1990). Bleaching in coral reef anthozoans: effects of irradiance, ultraviolet radiation, and temperature on the activities of protective enzymes against active oxygen. *Coral Reefs*, *8*(4): 225-232.

Lewis, E., Wallace, D., & Allison, L.J. (1998). *Program developed for CO_2 system calculations*. Carbon Dioxide Information Analysis Center, managed by Lockheed Martin Energy Research Corporation for the US Department of Energy.

Li, Y.H., & Gregory, S. (1974). Diffusion of ions in seawater and in deep-sea sediments. *Geochimica et Cosmochimica Acta*, *38*: 703–714.

Mackenzie, F.T., Bischoff, W.D., Bishop, F.C., Loijens, M., Schoon- Maker, J., & Wollast, R. (1983). Mg-calcites: low temperature occurrence, solubility and solid-solution behavior. In: Reeder, R.J. (Ed.), Reviews in Mineralogy, Carbonates: Mineralogy and Chemistry. Mineralogical Society of America, pp. 97–143.

Mackenzie, F.T., Lerman, A., & Ver, L.M. (2001). Recent past and future of the global carbon cycle. In: Gerhard LC, Harrison WE, Hanson BM (eds) Geological perspectives of global climate change. AAPG Studies in Geology #47, Tulsa, pp 51–82.

Marubini, F., Ferrier–Pages, C., & Cuif, J.P. (2003). Suppression of skeletal growth in scleractinian corals by decreasing ambient carbonate-ion concentration: a cross-family comparison. *Proceedings of the Royal Society of London. Series B: Biological Sciences*, *270*(1511): 179-184.

McGillis, W.R., Langdon, C., Loose, B., Yates, K.K., & Corredor, J.E. (2011). Productivity of a coral reef using boundary layer and enclosure methods. *Geophysical Research Letters*, *38*(3): 2–6. doi:10.1029/2010GL046179.

Mehrbach, C., Culberson, H., Hawley, J.E., Pytkowicz, R.M. (1973). Measurement of the apparent dissociation constants of carbonic acid in seawater at atmospheric pressure. *Limnology and Oceanography*, *18*: 897-907.

Miller, J., Muller, E., Rogers, C., Waara, R., Atkinson, A., Whelan, K.R.T., ... & Witcher, B. (2009). Coral disease following massive bleaching in 2005 causes 60% decline in coral cover on reefs in the US Virgin Islands. *Coral Reefs*, *28*(4): 925-937.

Millero, F., Feistel, R., Wright, D., & Mcdougall, T. (2008). The composition of Standard Seawater and the definition of the Reference-Composition Salinity Scale. Deep Sea Research Part I: *Oceanographic Research Papers 55*(1): 50–72.

Mills, A.L. (1999). The role of bacteria in environmental geochemistry. *The environmental geochemistry of mineral deposits. Reviews in Economic Geology, SEG, Littleton, CO. USA.(6A)*: 125-132.

Morell, J.M., & Corredor, J.E. (2001). Photomineralization of fluorescent dissolved organic matter in the Orinoco River plume: Estimation of ammonium release. *Journal of Geophysical Research: Oceans (1978–2012)*, *106*(C8): 16807-16813.

Morelock, J., Ramírez, W.R., Bruckner, A.W., & Carlo, M. (2001). Status of coral reefs, southwest Puerto Rico. *Caribbean Journal of Science, special publication*, *4*: 57.

Morelock, J., Schniedermann, N., & Bryant, W.R. (1977), Shelf reefs, southwestern Puerto Rico, in Reefs and Related Carbonates—Ecology and Sedimentology, AAPG Stud. Geol., 4: 135–153.

Morse, J., Andersson, A., & Mackenzie, F. (2006). Initial responses of carbonate-rich shelf sediments to rising atmospheric pCO_2 and "ocean acidification": Role of high Mg-calcites. *Geochimica et Cosmochimica Acta*, *70*(23): 5814–5830. doi:10.1016/j.gca.2006.08.017.

Morse, J.W., & Mackenzie, F.T. (1990). *Geochemistry of Sedimentary Carbonates*. *Clays and Clay Minerals* (pp. 1–725). Elsevier B.V.

Mucci, A. (1983). The solubility of calcite and aragonite in seawater at various salinities, temperatures, and one atmosphere total pressure. *American Journal of Science*, *283*(7): 780-799.

Navarro, A., Corredor, J. E., Morell, J., & Armstrong, R. (2000). Distribution of the cyanophyte Trichodesmium (Oscillatoriaceae) in the eastern Caribbean Sea: Influence of the Orinoco River. *Revista de biologia tropical*, *48*(Supl 1): 115-124.

Nesterenko, E.P., Nesterenko, P.N., Paull, B., Meléndez, M., & Corredor, J.E. (2012).Fast direct determination of strontium in seawater using high-performance chelation ion chromatography. *Microchemical Journal*.doi.org/10.1016/j.microc.2012.09.003.

Nesterenko, P.N., & Jones, P. (2007). Recent developments in the high-performance chelation ion chromatography of trace metals. *Journal of separation science 30*(11): 1773–93.

Olson, E.J., & Chen, C.T.A. (1982). Interference in the determination calcium in seawater. *Limnology and Oceanography*, *27*(2): 375–380.

Orr, J.C., Fabry, V.J., Aumont, O., Bopp, L., Doney, S.C., Feely, R.A., ... & Yool, A. (2005). Anthropogenic ocean acidification over the twenty-first century and its impact on calcifying organisms. *Nature*, *437*(7059): 681-686.

Pierrot, D., Lewis, E., & Wallace, D.W.R. (2006). MS Excel Program Developed for CO_2 System Calculations. ORNL/CDIAC-105. Carbon Dioxide Information Analysis Center, Oak Ridge National Laboratory, U.S. Department of Energy, Oak Ridge, Tennessee.

Precht, E., & Huettel, M. (2004). Rapid wave-driven advective pore water exchange in a permeable coastal sediment. *Journal of Sea Research*, *51*(2): 93–107. doi:10.1016/j.seares.2003.07.003.

Reeder, R.J. (1983). Crystal chemistry of the rhombohedral carbonates. In: Reeder RJ (ed) Carbonates: mineralogy and chemistry. Reviews in Mineralogy, Vol 11. Mineralogical Society of America, Washington, DC, p 1–47.

Reimers, C.E., Stecher III, H.A., Taghon, G. L., Fuller, C. M., Huettel, M., Rusch, A., ... & Wild, C. (2004). In situ measurements of advective solute transport in permeable shelf sands. *Continental Shelf Research*, *24*(2): 183-201.

Ribou, A.C., Salmon, J.M., Vigo, J., & Goyet, C. (2007). Measurements of calcium with a fluorescent probe Rhod-5N: Influence of high ionic strength and pH. *Talanta*, *71*(1): 437-442.

Rusch, A., & Huettel, M. (2000). Advective particle transport into permeable sediments-evidence from experiments in an intertidal sandflat. *Limnology and Oceanography*, *45*(3): 525-533.

Ruttimann, J. (2006). Oceanography: sick seas. *Nature*, *442*(7106): 978-980.

Sabine, C.L., Feely, R.A., Gruber, N., Key, R.M., Lee, K., Bullister, J. L., ... & Rios, A.F. (2004). The oceanic sink for anthropogenic CO_2. *Science*, *305*(5682): 367-371.

Sosa, A. (2012). Ciclo de 6202 días del seiche extremo en Isla Magueyes. 9 pp.1.43.

Stanley, S.M., Ries, J.B., & Hardie, L.A. (2002). Low-magnesium calcite produced by coralline algae in seawater of Late Cretaceous composition. *Proceedings of the National Academy of Sciences*, *99*(24): 15323-15326.

Sugrue, E., Nesterenko, P., & Paull, B. (2003). Iminodiacetic acid functionalised monolithic silica chelating ion exchanger for rapid determination of alkaline earth metal ions in high ionic strength samples. *The Analyst*, *128*(5) 417–420.

Sugrue, E., Nesterenko, P., & Paull, B. (2004). Ion exchange properties of monolithic and particle type iminodiacetic acid modified silica. *Journal of Separation Science*, *27*(10-11): 921–930.

The Royal Society. (2005). Ocean Acidification Due to Increasing Atmospheric Carbon Dioxide, Policy Document 12/05 (The Royal Society, London).

Traganza, E.D., & Szabo, B.J. (1967). Calculation of calcium anomalies on the Great Bahama Bank from alkalinity and chlorinity data. *Limnology and Oceanography, 12*(2): 281–286.

Ullman, W.J., & Aller, R.C. (1982). Diffusion coefficients in near-shore marine sediments. *Limnology and Oceanography*, *27*(3): 552-556.

Wanninkhof, R. (1992). Relationship Between Wind Speed and Gas Exchange Over the Ocean. *Journal of Geophysical Research*, *97*(C5): 7373–7382. doi:10.1029/92JC0018.

Weiss, R. (1974). Carbon dioxide in water and seawater: the solubility of a non-ideal gas. *Marine Chemistry*, *2*(3): 203-215.

Yates, K.K., & Halley, R.B. (2003). Measuring coral reef community metabolism using new benthic chamber technology. *Coral Reefs*, *22*(3): 247–255. doi:10.1007/s00338-003-0314-5.

Yates, K. K., & Halley, R. B. (2006). CO_3^{2-} concentration and pCO_2 thresholds for calcification and dissolution on the Molokai reef flat, Hawaii. *Biogeosciences*, *3*(3): 357-369.

Zeebe, R. E., & Wolf-Gladrow, D. (2001). *CO_2 in Seawater: Equilibrium, Kinetics, Isotopes: Equilibrium, Kinetics, Isotopes* (Vol. 65). Elsevier Science.

Appendix 1: Direct chromatographic separation and quantification and magnesium in seawater and sediment porewaters

LIMNOLOGY
and
OCEANOGRAPHY: METHODS

Limnol. Oceanogr.: Methods 11, 2013, 466–474

Direct chromatographic separation and quantification of calcium and magnesium in seawater and sediment porewaters

Melissa Meléndez[1], Ekaterina P. Nesterenko[2,3], Pavel N. Nesterenko[2], and Jorge E. Corredor[1]*

[1]Department of Marine Sciences, University of Puerto Rico, Mayagüez Campus, Puerto Rico

[2]Australian Centre for Research on Separation Science (ACROSS), School of Chemistry, University of Tasmania

[3]Irish Separation Science Cluster (ISSC), National Centre for Sensor Research, Dublin City University, Glasnevin, Dublin, Ireland

Abstract

Direct analysis of Ca^{2+} and Mg^{2+} is required for accurate determination of metastable carbonate mineral phase saturation states ($\Omega CaCO_3$; $\Omega MgCO_3$) in seawater, sediment porewaters, and other high ionic strength brines. To this end, we have implemented a method using High Performance Chelation Ion Chromatography *(HPCIC)* in which metal ion complexation at the stationary phase renders separation efficiency insensitive to high ionic strength matrix effects common to other ion chromatography (IC) methods. This method, using direct automated on-column injection, vastly increases sample throughput capacity in comparison to current titration methods. Calcium and magnesium ions in IAPSO standard seawater were selectively separated using a monolithic silica column (100 × 4.6 mm ID) activated with a covalently bonded iminodiacetic acid (IDA) chelator. The colored ion complexes resulting from post-column reaction (PCR) of the ions with a metallochromic indicator, in this case 4-(2-pyridylazo)-resorcinol (PAR), were detected spectrophotometricaly at 510 nm. Optimization of flow rate, eluent concentration, pH, and sample injection volume allowed baseline separation of Mg^{2+}(0.05474 mol kg^{-1}) and Ca^{2+} (0.01065 mol kg^{-1}) in less than 8 min using 2 μL seawater sample injections. At a flow rate of 1 mL min^{-1}, peak elutions occurred respectively at 4 and 5 min, using an eluent containing 0.1 M potassium chloride and 1 mM nitric acid adjusted to pH 2.5. Retention time variability below 0.5% for both metals following more than 200 injections indicates long-term stability of the derivatized monolithic silica column. Method application to marine sediment porewaters is discussed.

Accurate determination of $Mg^{2+}$and Ca^{2+} ion concentrations and their relative proportions in seawater, marine sediment porewaters and other environmental high ionic strength brines is troublesome despite their high concentrations due to the complexities of the matrix and chemical similarity which results in their co-precipitation (Traganza and Szabo 1967; Carpenter and Manella 1973; Kanamori and Ikegami 1980). Although $Mg^{2+}$and Ca^{2+} ion concentrations in open ocean waters are largely conservative with respect to salinity, coastal processes including biogenic and abiogenic precipitation, as well as carbonate sediment dissolution, can result in deviations from this norm (Gledhill 2005; Ribou et al. 2007). During carbonate precipitation from seawater, Mg^{2+} for example, can co-precipitate with Ca^{2+} yielding high-magnesium calcite thereby altering the Ca^{2+}/Mg^{2+} ratio and the ion activity product relative to Mg-calcite mineral phases. These Mg-calcite mineral phases (low and high Mg-calcites) are not well understood due to problems involving the precision of measurements and uncertainty regarding the basic thermodynamic solubility and kinetic properties of these phases (Morse et al. 2006). Accurate determination of Mg^{2+} and Ca^{2+} ion concentrations can help elucidate such difficulties.

Changes in seawater saturation state (Ω) with respect to metastable carbonate phases are not only affected by changes in the seawater CO_3^{2-} concentration. Variations in the Mg^{2+} and Ca^{2+} ion seawater concentrations and their ratio imply changes in Mg-calcite composition and solubility, Mg content in marine calcifying organisms skeletons, as well as changes in seawater Ω (Andersson et al. 2008). The delicate equilibrium between these two alkaline earth metal cations is triggered by

*Corresponding author: E-mail: melissa.melendezoyola@upr.edu

Acknowledgments

Authors would like to give thanks to Drs. Dwight Gledhill and Andreas Andersson for their assistance and recommendations throughout this research. Special thanks are due to the research group at the Australian Centre for Research on Separation Science (ACROSS) and to Dr. Brett Paull at University of Tasmania, Australia. Support for this study was provided, in part, by the Caribbean Coastal Ocean Observing System (CariCOOS), NOAA Coral Reef Conservation Program, Puerto Rico Sea Grant College Program, ExxonMobil, Department of Marine Science UPR-M and ACROSS.

DOI 10.4319/lom.2013.11.466

slight changes in alkalinity and carbon dioxide tension that may cause their precipitation or dissolution (Laurence 1926; Brewer et al. 1975). In sediment porewaters, changes in Ca^{2+}, Mg^{2+}, and CO_3^{2-} concentrations arise from the precipitation or dissolution of calcium carbonate minerals (Koczy 1956; Traganza and Szabo 1967; Kanamori and Ikegami 1980; Kleypas et al. 2006; Ribou et al. 2007). The direct quantification of the Mg^{2+} and Ca^{2+} seawater ion concentrations can help in understanding the chemical behavior of seawater metastable carbonate mineral phases and in more accurate determination of their corresponding seawater Ω (Kleypas et al. 2006; Ribou et al. 2007).

Current methods for the determination of Mg^{2+} and Ca^{2+} ion concentrations in seawater use gravimetric procedures and ion-exchange separation combined with titration methods. Due to the precision difficulties, seawater Mg^{2+} ion concentration is usually determined as the difference between total alkaline earth metals and Ca^{2+} plus strontium (Kanamori and Ikegami 1980). Meanwhile Ca^{2+} is selectively titrated with Zincon (Zn- ethylene glycol-bis(2-aminoethylether)-N,N,N′,N′-tetraacetic acid [EGTA]) (Culkin and Cox 1976; Kanamori and Ikegami 1980), ethylenediamine-N,N,N′,N′-tetraacetic acid (EDTA) (Riley and Tongudai 1967), or glyoxal-bis(2-hydroxyanil) (GBHA) (Tsunogai et al. 1968). Other methods incorporate ion selective electrodes as end-point indicators (Whitfield et al. 1969; Růžička et al. 1973; Lebel and Poisson 1976; Kanamori and Ikegami 1980). These methods are laborious and time-consuming, and as a result, sample throughput is limited in the best cases to a few tens of sample analyses per day. Additionally, most of these techniques do not have sufficient resolution to detect the small changes due to calcification processes. A direct in situ method using a custom-made ion-selective electrode has been described (Wenzhöfer et al. 2001), but resolution is poor and the electrode is not commercially available. Other instrumental methods include inductively coupled plasma spectrometry (ICP-MS), atomic absorption spectrophotometry (AAS), and flame atomic absorption spectrophotometry (FAA). However sample pretreatment is needed, interferences from other major ionic components in the matrix are expected, and analysis costs can be high.

Recently, chromatographic techniques have been developed that can provide higher energy interactions between the ionic analytes of interest and selected adsorbents or stationary phases increasing significantly the degree of separation selectivity. Chelation ion chromatography (CIC), first described by Moyers and Fritz in 1977, is a retention mechanism that allows specific interactions between a dissolved metal ion analyte and a chelating stationary phase. Paull et al. (1996) demonstrated the potential application of CIC to the problem of Mg^{2+} and Ca^{2+} ion separation using a dynamic chelating ion exchange mechanism whereby a chelator dissolved in the carrier coats a porous graphitic carbon column. In recent developments, selected organic ligands covalently bonded to inert substrates serve as the stationary phase. Metal ion analytes form very stable complexes with these ligands and hence efficient separation is achieved (Nesterenko et al. 2011; Nesterenko et al. 2013).The use of chelating ion-exchangers to form kinetically labile surface complexes and retain metal ions according to the stability of corresponding complexes is one of the multiple advantages in high performance liquid chelation ion chromatography (HPLCIC) (Nesterenko and Jones 2007). Modification of monolithic silica columns with covalently bonded chelating iminodiacetic acid (IDA) groups has proven to allow excellent cation separation and increased peak efficiencies compared with other columns.

We here describe implementation of an HPLCIC method for separation and quantification of Mg^{2+} and Ca^{2+} ions in seawater in less than 8 min. We use a monolithic silica column derivatized with a covalently bonded IDA chelator for separation, and post-column derivatization of the ions with 4-(2-pyridylazo)-resorcinol (PAR) for optical detection and quantification. The metallochromic reagent PAR forms water-soluble complexes with Mg^{2+} and Ca^{2+} ions of moderate molar absorptivities (~ 10^4 at about 500 nm), therefore exhibiting robust sensitivity for spectrophotometric detection (Jezorek and Freiser 1979). Monolithic HPLC columns, employing a continuous silica matrix etched with porous channels, surpass traditional packed bead column performance with higher separation efficiency, reduced retention times, and low column backpressure.

Benefits of this method include elimination of the need for sample pretreatment or manipulation, high sample throughput achievable with automated sample injection, low sample volume required, reduced number of solutions necessary, lack of interference from other ionic compounds, method simplicity and reliability, and reduced sensitivity to the ionic strength of the sample matrix. Whereas we have yet to achieve the canonical precision of 0.1% quoted for seawater applications (Carpenter and Manella 1973; Kanamori and Ikegami 1980; Olson and Chen 1982), the method can currently be applied to sediment porewaters and further method refinement is expected to achieve this requirement.

To explore anticipated improvement in method reproducibility with increased injection volume but given limitation to seawater Ca^{2+} and Mg^{2+} analysis imposed by column-loading capacity and detector saturation, we performed a series of experiments using increasing injection volumes of Mn^{2+} ion proxy at low concentration. Manganese ion was chosen because it exhibits greater molar absorptivity with the PAR reagent allowing use of more dilute and less acidic solutions.

Materials and procedures

Monolithic silica IDA modified column

A monolithic bare silica column (Phenomenex 100 × 4.6 mm) was modified with IDA chelator through the activation of silanol groups at the surface of the silica monolith column with distilled water at 60°C followed by recycling of mixture

IDA and 3-glycidoxypropyltriethoxysilane through the column at 70°C (for method details see Sugrue et al. 2003; Nesterenko and Jones 2007; Nesterenko et al. 2013). Surface treatment and functionalization of the continuous unitary porous structure and structure of the bonded layer within such columns have been described by Sugrue et al. (2004) and Nesterenko et al. (2013).

Reagents and solutions

For photometric detection, we used PAR reagent (CAS# 1141-59-9, acid form – Fluka, 99% purity) as a post-column reagent. We prepared stock solutions of 1 mM PAR and 2 M ammonium hydroxide (analytical reagent grade). The high pH of the stock solution prevents adsorption onto plastic surfaces. The standard post column reagent was prepared by dilution to 0.05 mM PAR. To adjust the pH to ~ 10.4, we used 2 M nitric acid (analytical reagent grade). The post-column reagent thus prepared is stable for weeks if not months, and will not need filtering, degassing, or an overpressure of inert gas.

The mobile phase was prepared using 0.1 M potassium chloride (KCl) and 1 mM HNO_3, pH of ~ 2.5. Standard seawater (International Association for the Physical Sciences of the Ocean – IAPSO, batch 149; 10 May 2007) with salinity 34.994 was purchased from OSIL (Havant, UK). Stoichiometric reference composition of IAPSO standard seawater provides the best current estimation of Mg^{2+} (0.05474 mol kg^{-1}) and Ca^{2+} (0.01065 mol kg^{-1}) concentrations in seawater (Millero et al. 2008).

We used Nalgene bottles for storage of all stock and working solutions due to their low metal contamination. Glassware and plasticware were acid washed before use with 10 mL of 1 M nitric acid followed by a rinse with deionized water provided form a Milli-Q system (Millipore, Bedford, USA).

Chromatographic instrumentation

A Waters 2695 HPLC Separations Module (Waters, Milford, MA, USA) chromatography system was used. The autosampler built in to the Separation Module allowed runs of 178 samples in a single analytical sequence. Column oven was set to 30°C for all separations. A post column reaction (PCR) flow system was used to allow cation detection. The 1/16″ polypropylene mixing coil used in the PCR was about 2.5 m long using a high-pressure pump (Model 350 Scientific System Inc.). The colored PAR-derivatized cations were detected spectrophotometricaly using a model 2487 UV/VIS spectrophotometric detector operated at 510 nm. Data were processed using the Waters Empower 3 Software.

Porewater samples

Stainless steel well samplers (3/4-inch ID) were developed, which allow porewater sampling down to 20 cm sediment depth. Each sampler is placed 1 m apart on a 10 m transect along the reef. Each sampling port consists of thirty 1/16-inch holes drilled around the sample in a 1 cm span. Samples were taken at 2 cm resolution through the upper 20 cm of the sediment column. Following the technique described by Falter and Sansone (2000), we installed the samplers by first hammering a stainless steel tube (54 cm long, 5/8-inch ID) into the sediment and then replacing it with the well sampler. After insertion into the sediment, the sampler was left on site allowing repetitive sampling at identical locations and depth intervals. Porewater samples were collected in situ by withdrawing porewater using two 60 cc syringes and storing in 125 mL plastic sample bottles. Each sample was filtered through 0.45 μm membrane filters and poisoned with 60 μL of a saturated $HgCl_2$ solution to prevent biological alteration of the sample. Porewater salinity was determined using the Guildline Autosal 8400B salinometer with a precision of ± 0.003. Conductivity, Temperature, and Depth (CTD) casts of the overlying water column were routinely performed. Surface and bottom samples of the overlying seawater were collected for analyses as well using a Van Dorn bottle.

Assessments

Optimization of the method

We tested eluent concentration over ranges of 0.1 to 0.5 M KCl and 1 to 4 mM HNO_3 with pH between 2.5 and 3.0. Baseline cation separation and peak shape were found to be optimal at 0.1 M of KCl and 1 mM HNO_3. Systematic reduction of HNO_3 and KCl concentrations improved the response and produced sharper and narrower peak shapes. These optimized eluent concentrations allowed return to baseline between peaks for up to 0.5 s. Variations in eluent pH from 2 to 3 were tested, but no significant changes in retention or peak shapes were observed.

The effect on reaction completion of varying PCR reagent flow rate was tested. Increasing PCR reagent flow rate from 0.7 to 1 mL min^{-1} resulted in increased photometric response for both analytes in standard seawater (Fig. 1). Maximum absorbance response was obtained at a flow rate of 1 mL min^{-1}. To minimize the ambiguities introduced in addressing both the reagent and eluent delivery proportions, absorbance

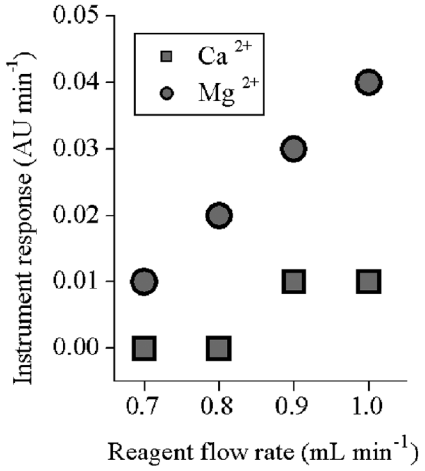

Fig. 1. Effect of PCR reagent flow rates on Ca^{2+} and Mg^{2+} responses using standard seawater as a probe. Maximum absorbance response is observed at 1 mL min^{-1}.

response was investigated through standard addition (Sugrue et al. 2003). Reagent flow rates tested ranged from 0.5 to 1 mL min^{-1}. Table 1 shows the changes in linear regression coefficients with variation of PCR flow rate of Mg^{2+} and Ca^{2+} ions. Peak absorbance exhibits a linear relationship with Ca^{2+} ion concentration (R^2 = 0.99, n = 8) at reagent flow rate of 0.5 mL min^{-1}, but Mg^{2+} is incompletely derivatized at this low reagent flow rate. The correlation coefficient for magnesium increased significantly with increased reagent flow rate. Highest linear correlation between reagent flow rate and absorbance response for Mg^{2+} was achieved at 0.9 mL min^{-1} (R^2 = 0.98, n = 10). Despite a modest concurrent Ca^{2+} coefficient decrease from 0.99 to 0.95, this does not significantly compromise analyte determination. Fig. 2 shows the dependence of response against concentration of both metals using different standard addition concentrations of Mg^{2+} and Ca^{2+}, at 1 mL min^{-1} eluent flow rate and 0.9 mL min^{-1} PCR reagent flow rate.

Table 1. Coefficients of determination of linear regressions (R^2) of Mg^{2+} and Ca^{2+} standard concentrations versus absorbance at different reagent flow rates using standard additions.

Reagent flow rate (mL min^{-1})	R^2 Mg^{2+}	R^2 Ca^{2+}
0.5	0.05	0.99
0.6	0.23	0.97
0.7	0.51	0.96
0.8	0.73	0.82
0.9	0.98	0.95

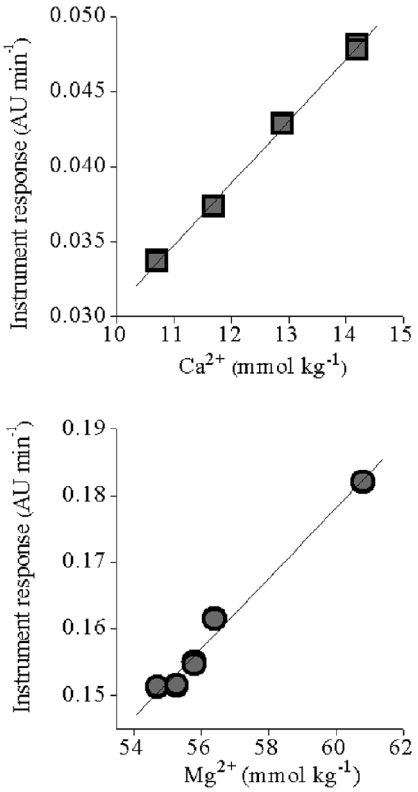

Fig. 2. Linearity of Ca^{2+} (R^2 = 0.99, n = 8) and Mg^{2+} (R^2 = 0.98, n = 10) standard addition at reagent flow rate of 0.9 mL min^{-1}. Standards were measured in duplicate.

Effect of sample injection volume was tested for 2, 5, and 10 μL by assessing replicate reproducibility of three standard seawater injections (n = 9). Increasing sample volume resulted in lower reproducibility as shown by the increased standard deviation of peak areas (Fig. 3). Response reproducibility was best with smallest injected volume of the sample. Injection volume of 2 μL was consequently selected for routine operation.

Increased detector response with increased PRC reagent flow rate, but the absence of plateaus for either Ca^{2+} or Mg^{2+} (Fig. 1), indicates that post-column reaction completion was not reached even at the highest flow rate possible (1 mL min^{-1}). These circumstances result in limited method reproducibility despite intentional minimization of injection volume to the smallest injection loop possible (1 mL).

To explore the effect of varying sample injection volume on reproducibility using the Mn^{2+} ion proxy (given the column loading limitation for Ca^{2+} and Mg^{2+} ions) at a concentration of 45.5 nM prepared from standard 1000 ppm in 0.5 M nitric acid, we performed 10 consecutive runs each for 2, 4, 10, and 20 μL injection volumes keeping column temperature and sample temperature constant at 25°C. The eluent used in this test was slightly different (3 mM HNO_3; 0.1 M KCl) from that used for seawater Mg^{2+} and Ca^{2+} analysis to minimize run time. The post column reagent was as previously described delivered at 0.9 mL min^{-1}. Increased injection volume using the Mn^{2+} ion proxy resulted in reduction of the relative standard deviation (RSD) from 4.8% at 2 μL injection volume to 0.7% at 20 μL injection volume (Fig. 4).

Method performance following optimization

A chromatogram performed under optimized parameters using the IDA-modified silica monolithic column shows com-

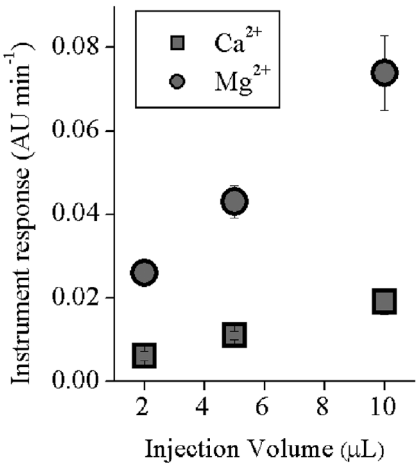

Fig. 3. Effect of sample volume injection on relative instrument response.

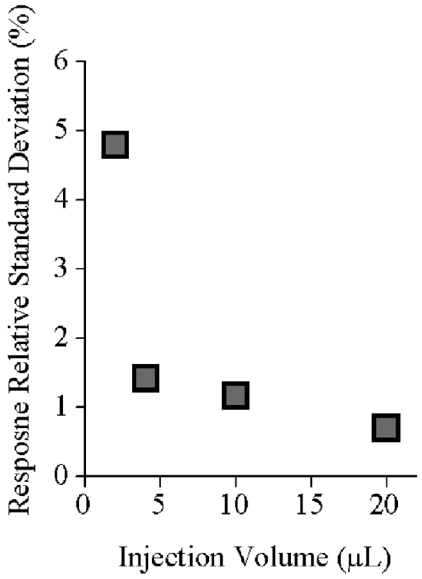

Fig. 4. Effect of increasing sample injection volumes on method reproducibility using Mn^{2+} metal as an ion proxy.

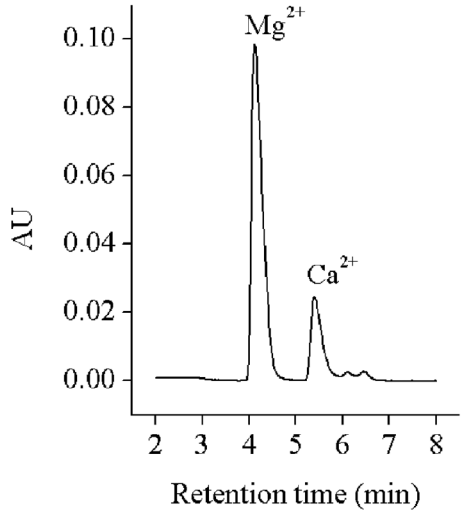

Fig. 5. Chromatogram of Mg^{2+} and Ca^{2+} in standard seawater obtained using eluent of 0.1 M of KCl and 1 mM of HNO_3 at pH ~ 2.5, flow-rate, 1.0 mL min^{-1}; sample injection volume, 2 μL; PCR 0.05 mM PAR at pH ~ 10.4, flow rate, 0.9 mL min^{-1}; photometric detection at 510 nm.

plete baseline separation of Mg^{2+} and Ca^{2+} ions in standard seawater achieved in less than 8 min at a flow rate of 0.9 mL min^{-1} (Fig. 5). Column efficiencies calculated from chromatographic peaks are 13,720 and 24,800 theoretical plates per meter for Mg^{2+} and Ca^{2+}, correspondingly. These numbers are in a good agreement with values ranging 18,000 to 37,560 reported for such columns (Sugrue et al. 2003). The difference in efficiency calculated for the massive Mg^{2+} peak is connected with partial overloading of the column, which caused some peak broadening. Although increased eluent flow rate can

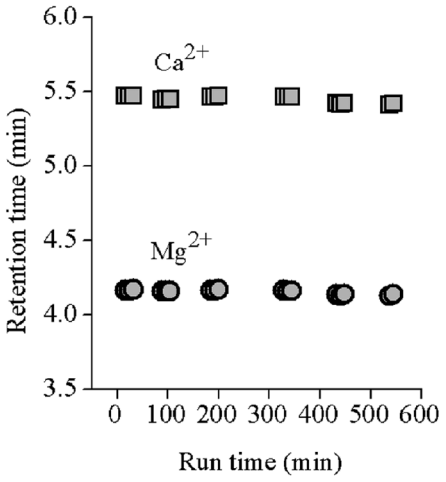

Fig. 6. Column stability as indicated by retention time consistency for Mg^{2+} and Ca^{2+} in standard triplicate seawater samples analyzed following every ~ 30 porewater sample injections.

deliver separation in a period of less than 4 min, selectivity, peak symmetry, and resolution of the massive Ca^{2+} and Mg^{2+} peaks in our samples are favored at the lower flow rate with the higher retention time.

Retention time variability was used to assess long-term column stability. During operational runs, a sample of standard seawater was analyzed every ~ 30 injections. Twenty-one samples of standard seawater were analyzed through the sequence of 60 sediment porewater samples. The average retention times were 4.15 ± 0.01 min for Mg^{2+} and 5.44 ± 0.02 min for Ca^{2+}. Retention time variability over the 656 min (10.9 h) of consecutive injections was 0.4% and 0.5%, respectively, for Mg^{2+} and Ca^{2+} (Fig. 6).

Throughout a sequence of 243 consecutive sample injections, the maximum variability from the stoichiometric reference composition of standard seawater defined by Millero et al. (2008) (Mg^{2+} 0.05474 mol kg^{-1} and Ca^{2+} 0.01065 mol kg^{-1}) was 1% for Mg^{2+} and 2% for Ca^{2+} (Fig. 7 and Table 2).

Determination of Mg and Ca in sediment porewaters

Example of method application

The optimized HPCIC method enabled analysis of high ionic strength seawater and porewaters samples. Vertical distribution and temporal variability of Mg^{2+} and Ca^{2+} in sediment porewaters collected at a mid-shelf reef off La Parguera, Puerto Rico, from June to September 2011 was examined. We analyzed a series of 60 samples in triplicate (180 injections) under optimized conditions as described above. Average RSD for triplicate samples was 1% and 2%, respectively, for Mg^{2+} and Ca^{2+} ions. The maximum and the minimum RSD registered for one sample in triplicate was 2% and 7% and 0.1% and 0.2%, respectively, for Mg^{2+} and Ca^{2+} ions.

In general, Mg^{2+} and Ca^{2+} sediment porewater concentrations at Enrique Reef increased with depth in the sediment column. Whereas temporal changes are apparent, no definite tem-

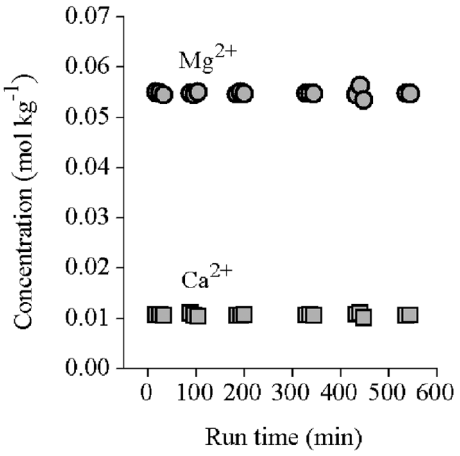

Fig. 7. Column stability as indicated by the concentration of Mg^{2+} and Ca^{2+} in standard seawater analyzed following every ~ 30 porewater sample injections.

poral trend was evident (Fig. 8).The maximum increases over sediment-water interface surface values to 16 cm depth within the sediment were 0.0063 and 0.0038 mol kg^{-1} for Mg^{2+} and Ca^{2+}, respectively. These changes with depth are large relative to the measurement error. Porewater Mg^{2+}/Ca^{2+} ratios decreased with depth presumably as a result of sediment dissolution of metastable carbonate phases. Maximum and minimum Mg^{2+}/Ca^{2+} ratios were 5.37 and 4.22, respectively (Fig. 9).

Discussion

The method here described optimizes chelation-based separation of the alkaline earth metal ions Mg^{2+} and Ca^{2+} at high concentrations on the monolithic IDA column using a high ionic strength/low pH eluent. The method makes possible rapid automated analysis of Mg^{2+} and Ca^{2+} in high ionic strength matrices such as marine sediment porewaters.

Completion of the post-column complexation reaction with the colored reagent posed an analytical challenge due to the high concentration of Mg^{2+} and Ca^{2+}, third and fourth most abundant ions in seawater. Magnesium was a particular challenge because of its high concentration in seawater and mainly because of its short residence time in the chromatographic column. The latter factor means that the Mg^{2+} band migrates through a significant part of the chromatographic column together with the massive band of alkali metal cations from seawater resulting in column overloading and peak broadening. Kinetically, complex formation with PAR was "fast." Increasing the PCR reagent delivery allowed the complexes to form through the post-column reaction. This process is apparent in the resulting chromatogram (Fig. 5), which because of the fast kinetics of chelate formation and dissociation shows relatively narrow peak shapes.

Column efficiency was not compromised throughout the analytical run of 243 samples, and no significant variability of retention times was observed (see Fig. 6). The use of covalently bonded chelating reagents in the stationary phase of the monolithic column reduced the necessity for dilution, sample pretreatment, or the use of multi-column separation techniques. The high retention of Mg^{2+} and Ca^{2+} on the surface monolithic phase is evident. The column can be used to analyze other alkaline earth metals, such as Sr^{2+} and Ba^{2+} in samples containing excess Mg^{2+} and Ca^{2+} (Sugrue et al. 2003; Nesterenko et al. 2013).

The method using the IDA-modified silica monolithic column described in this study offers new possibilities to gain meaningful insight into the biogeochemical processes occurring in permeable sediments. Organic matter remineralization processes and the concomitant metabolic CO_2 production force carbonate dissolution in aerobic surface layers of the calcareous marine sediments resulting in increased Mg^{2+} and Ca^{2+} concentrations at depth within the sediment (Burdige and Zimmerman 2002; Andersson et al. 2006). Direct porewater Mg^{2+} and Ca^{2+} ion measurements provide additional evidence for the occurrence of sediment carbonate dissolution and can be used to address the question of preferential dissolution of metastable carbonate phases (Mackenzie et al. 1983; Morse et al. 1985, 2006; Burdige and Zimmerman 2002).

System limitations for handling the massive alkaline earth cation concentrations of seawater remain. Addressing the

Table 2. Variability of apparent Mg^{2+} and Ca^{2+} ion concentrations and ionic ratio in standard seawater (SSW) analyzed throughout the porewater sample analysis run. Percent difference from Mg^{2+} and Ca^{2+} ion concentrations in standard seawater as established by Millero et al. (2008).

n	[Mg^{2+}] (mol kg^{-1})	[Ca^{2+}] (mol kg^{-1})	% Delta Mg^{2+} to SSW	% Delta Ca^{2+} to SSW
1	0.0550	0.0107	0	0
2	0.0548	0.0107	0	0
3	0.0544	0.0106	–1	–1
4	0.0547	0.0111	0	4
5	0.0545	0.0105	0	–1
6	0.0550	0.0104	0	–3
7	0.0546	0.0106	0	–1
8	0.0550	0.0106	0	0
9	0.0547	0.0108	0	1
10	0.0548	0.0107	0	0
11	0.0547	0.0107	0	0
12	0.0547	0.0106	0	–1
13	0.0545	0.0108	0	1
14	0.0563	0.0110	3	3
15	0.0534	0.0102	–2	–4
16	0.0548	0.0106	0	0
17	0.0547	0.0107	0	0
18	0.0549	0.0106	0	0
19	0.0546	0.0106	0	0
20	0.0547	0.0107	0	1
Avg	0.0547	0.0107	0	0
SD	0.0005	0.0002	1	2

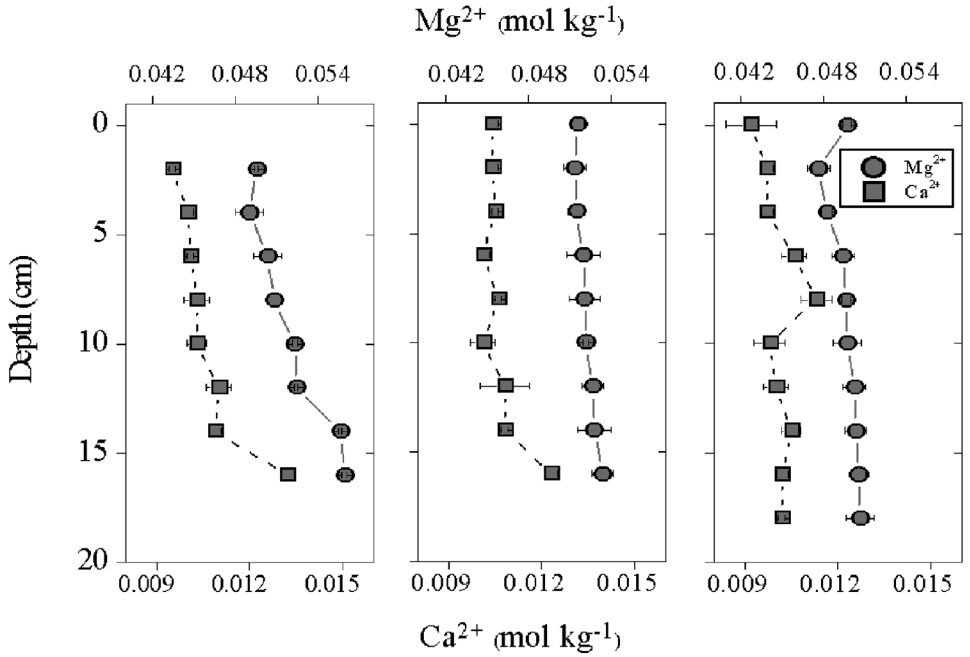

Fig. 8. Vertical porewater profiles for Mg^{2+} and Ca^{2+} ion concentration at Enrique Reef during June (left), July (center), and September 2011 (right).

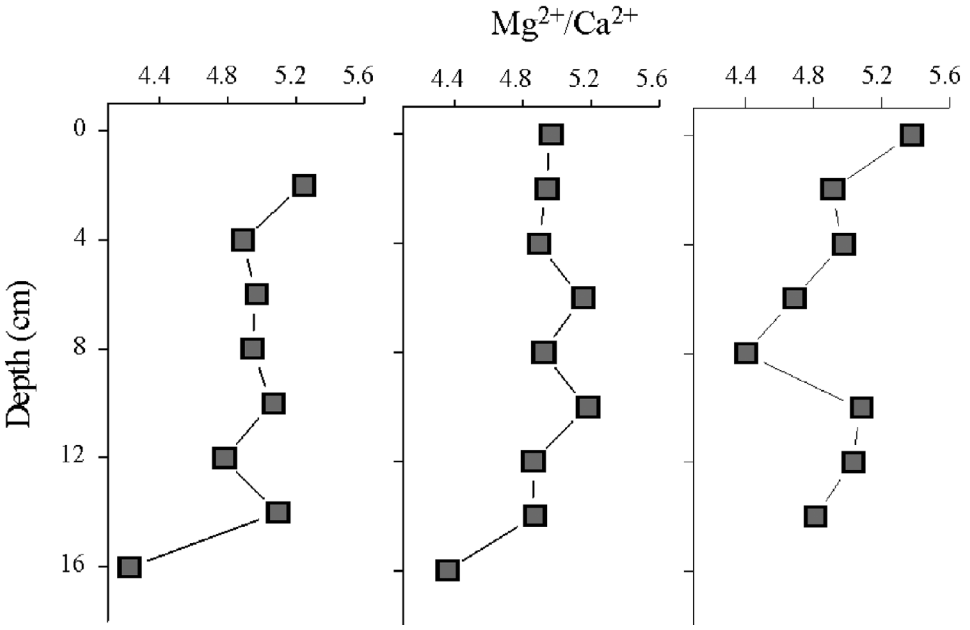

Fig. 9. Vertical porewater profiles for Mg^{2+}/Ca^{2+} ion ratios at Enrique Reef during June (left), July (center), and September 2011 (right).

"chemical" problems of column overload, detector saturation, and reaction completion by sample volume reduction resulted in the "mechanical" problem of poor injection reproducibility. To confirm the dependence of reproducibility on injection sample volume, we used a very dilute Mn^{2+} solution so as to assure operation within the linear range of the calibration plot. Dramatic improvement of reproducibility with larger injected volumes (up to 20 μL) (see Fig. 4) confirms the poor performance of low volume sample injection and points the way toward method optimization.

Comments and recommendations

Although the method as here presented is applicable to study large variations of Mg^{2+} and Ca^{2+} in marine sediment

porewaters, further improvement of method precision will be necessary for the determination of small changes in seawater. Observations of alkalinity changes indicate that calcification in coral reef environments can be expected to change Ca^{2+} concentration by less than ~ 0.050 mM over a daily cycle posing a considerable analytical challenge.

Accuracy of our analyses was compromised by the inability to reduce sample injection below 1 μL since we injected very concentrated samples into a column of internal diameter 4 mm. Our experiments with the Mn^{2+} ion proxy, however, demonstrate significant improvement of method reproducibility using greater injection volume (Fig.4). We consequently recommend the use of higher capacity columns (internal diameter 8 mm for example) to allow increasing sample volume injection to more reproducible volumes in the range of 10-20 μL. Auto sampler injection accuracy, in particular, increases substantially in this range.

Fully automated chromatographic analysis of Mg^{2+} and Ca^{2+} in seawater exhibits significant advantages over titration methods including rapid sample throughput, low sample volume, and decreased operator labor. A single chromatographic determination is 5 to10 times faster than the corresponding determination by titration. Although autotitrators can be equipped with autosamplers, sample volumes used are orders of magnitude higher than for HPCIC resulting in lower sample loading capacity. Because the cost of the basic equipment, reagents, and materials is comparable for both methods, chromatographic determination is more cost-effective, especially for large sample numbers.

References

Andersson, A. J., F. T. Mackenzie, and N. R. Bates. 2008. Life on the margin: implications of ocean acidification on Mg-calcite, high latitude and cold-water marine calcifiers. Mar. Ecol. Prog. Ser. 373:265-273 [doi:10.3354/meps07639].

———, F. T. Mackenzie, and A. Lerman. 2006. Coastal ocean CO_2–carbonic acid–carbonate sediment system of the Anthropocene. Glob. Biogeochem. Cycles 20(1):1-13 [doi:10.1029/2005GB002506].

Brewer, P. G., G. T. F. Wong, M. P. Bacon, and D.W. Spencer. 1975. An oceanic calcium problem? Earth Planet. Sci. Lett. 26(1):81-87 [doi:10.1016/0012-821X(75)90179-X].

Burdige, D. J., and R. C. Zimmerman. 2002. Impact of sea grass density on carbonate dissolution in Bahamian sediments. Limnol. Oceanogr. 47(6):1751-1763 [doi:10.4319/lo.2002.47.6.1751].

Carpenter, J. H., and M. E. Manella. 1973. Magnesium to chlorinity ratios in seawater. J. Geophys. Res. 78(18):3621-3626 [doi:10.1029/JC078i018p03621].

Culkin, F., and R. A. Cox. 1976. Sodium, potassium, magnesium, calcium and strontium in sea water. Deep Sea Res. Oceanogr. Abstr. 13(5):789-804 [doi:10.1016/0011-7471(76)90905-0].

Falter, J. L., and F. J. Sansone. 2000. Shallow porewater sampling in reef sediments. Coral Reefs 19(1):93-97 [doi:10.1007/s003380050233].

Gledhill, D. K. 2005.Calcite dissolution kinetics and solubility in Na-Ca- Mg-Cl brines of geologically relevant composition at 0.1 to 1 bar pCO_2 and 25 to 80°C. Ph.D. thesis, Texas A&M Univ.

Laurence, I. 1926. The precipitation of calcium and magnesium from sea water. J. Mar. Biol. Assoc. U.K. 14(02):441-446 [doi:10.1017/S002531540000792X].

Jezorek, J. R., and H. Freiser. 1979. 4-(Pyridylazo)resorcinol-based continuous detection system for trace levels of metal ions. Anal. Chem. 51(3):373-376 [doi:10.1021/ac50039a012].

Kleypas, J. A., R. A. Feely, V. J. Fabry, C. Langdon, C. L. Sabine, and L. L. Robbins. 2006. Impacts of ocean acidification on coral reefs and other marine calcifiers: A guide for future research, report of a workshop held 18-20 April 2005, St. Petersburg, FL, sponsored by NSF, NOAA, and the U.S. Geological Survey, p. 1-88.

Kanamori, S., and H. Ikegami. 1980. Computer-processed potentiometric titration for the determination of calcium and magnesium in seawater. J. Oceanogr. Soc. Japan 36(4):177-184 [doi:10.1007/BF02070330].

Koczy, F. F. 1956.The specific alkalinity. Deep Sea Res. 3(4):279-288 [doi:10.1016/0146-6313(56)90018-1].

Lebel, J., and A. Poisson. 1976. Potentiometric determination of calcium and magnesium in seawater. Mar. Chem. 4(4):321-332 [doi:10.1016/0304-4203(76)90018-9].

Mackenzie, F.T.,W. D. Bischoff, F.C. Bishop, M. Loijens, J. Schoonmaker, and R. Wollast. 1983. Mg-calcites: low temperature occurrence, solubility and solid-solution behavior, p. 97-143. *In* R. J. Reeder [ed.], Reviews in mineralogy, carbonates: Mineralogy and chemistry. Mineralogical Society of America.

Millero, F., R. Feistel, D.Wright, and T. Mcdougall. 2008. The composition of standard seawater and the definition of the reference-composition salinity scale. Deep Sea Res. I 55(1):50-72 [doi:10.1016/j.dsr.2007.10.001].

Morse, J., A. J. Andersson, and F. Mackenzie. 2006. Initial responses of carbonate-rich shelf sediments to rising atmospheric pCO_2 and "ocean acidification:" Role of high Mg-calcites. Geochim. Cosmochim. Acta 70(23):5814-5830 [doi:10.1016/j.gca.2006.08.017].

Morse, J. W., J. J. Zullig, L. D. Bernstein, F. J Millero, P. J. Milne, A. Mucci, and G. R. Choppin. 1985. Chemistry of calcium carbonate-rich shallow water sediments in the Bahamas. Am. J. Sci. 285(2):147-185 [doi:10.2475/ajs.285.2.147].

Moyers, E. M., and J. S. Fritz. 1977. Preparation and analytical applications of a propylenediaminetetraacetic acid resin. Anal. Chem. 49(3):418-423 [doi:10.1021/ac50011a023].

Nesterenko, E. P., P. N. Nesterenko, B. Paull, M. Meléndez, and J. E. Corredor. 2013. Fast direct determination of strontium in seawater using high-performance chelation ion chromatography. Microchem. J. 111:8-15 [doi:10.1016/j.microc.2012.09.003].

Nesterenko, P. N., and P. Jones. 2007. Recent developments in the high-performance chelation ion chromatography of trace metals. J. Separat. Sci. 30(11):1773-1793 [doi:10.1002/jssc.200700126].

———, P. Jones, B. Paull, and Royal Society of Chemistry (Great Britain). 2011. High performance chelation ion chromatography. *In* R. M. Smith [ed.], RSC Chromatographic Series, RSC Chemistry, Cambridge, 2011, p. 284–303 [doi:10.1039/9781849732314-00284].

Olson, E. J., and C.T. A. Chen. 1982. Interference in the determination calcium in seawater. Limnol. Oceanogr. 27(2):375-380 [doi:10.4319/lo.1982.27.2.0375].

Paull, B., P. A. Fagan, and P. R Haddad. 1996. Determination of calcium and magnesium in sea-water using a dynamically coated porous graphitic carbon column with a selective metallochromic ligand as a component of the mobile phase. Anal. Commun. 33(6):193-196 [doi:10.1039/ac9963300193].

Ribou, A. C., J. M. Salmon, J. Vigo, and C. Goyet. 2007. Measurements of calcium with a fluorescent probe Rhod-5N: Influence of high ionic strength and pH. Talanta 71(1):437-442 [doi:10.1016/j.talanta.2006.04.011].

Riley, J. P., and M. Tongudai. 1967. The major cation/chlorinity ratios in seawater. Chem. Geol. 2:263-269 [doi:10.1016/0009-2541(67)90026-5].

Růžička, J., E. H. Hansen, and J.C. Tjell. 1973. Selectrode—the universal ion-selective electrode: Part VI. The calcium(II) selectrode employing a new ion exchanger in a nonporous membrane and a solid-state reference system. Anal. Chim. Acta 67(1):155-178 [doi:10.1016/S0003-2670(01)80243-9].

Sugrue, E., P. Nesterenko, and B. Paull. 2003. Iminodiacetic acid functionalised monolithic silica chelating ion exchanger for rapid determination of alkaline earth metal ions in high ionic strength samples. Analyst 128(5):417-420 [doi:10.1039/b303467d].

———, P. Nesterenko, and B. Paull. 2004. Ion exchange properties of monolithic and particle type iminodiacetic acid modified silica. J. Separat. Sci. 27(10-11):921-930 [doi:10.1002/jssc.200401794].

Traganza, E. D., and B. J. Szabo. 1967. Calculation of calcium anomalies on the Great Bahama Bank from alkalinity and chlorinity data. Limnol. Oceanogr. 12(2):281-286 [doi:10.4319/lo.1967.12.2.0281].

Tsunogai, S., M. Nishimura, and S. Nakaya. 1968. Calcium and magnesium in sea water and the ratio of calcium to chlorinity as a tracer of water-masses. J. Oceanogr. Soc. Japan 24(4):153-159.

Wenzhöfer, F., M. Adler, O. Kohls, C. Hensen, B. Strotmann, S. Boehme, and H. Schulz. 2001. Calcite dissolution driven by benthic mineralization in the deep-sea: in situ measurements of Ca^{2+}, pH, pCO_2 and O_2. Geochim. Cosmochim. Acta 65(16):2677-2690 [doi:10.1016/S0016-7037(01)00620-2].

Whitfield, M., J. V. Leyendekkers, and J. D. Kerr. 1969. Liquid ion-exchange electrodes as end-point detectors in compleximetric titrations: Part II. Determination of calcium and magnesium in the presence of sodium. Anal. Chim. Acta 45(3):399-410 [doi:10.1016/S0003-2670(01)95569-2].

Submitted 24 January 2013
Revised 28 June 2013
Accepted 20 August 2013